arXiv:1609.01925v2 [astro-ph.HE] 15 Sep 2016

Large X-ray Flares on Stars Detected with MAXI/GSC: A Universal Correlation between the Duration of a Flare and its X-ray Luminosity

Yohko TSUBOI[1], Kyohei YAMAZAKI[1], Yasuharu SUGAWARA[1], Atsushi KAWAGOE[1], Soichiro KANETO[1], Ryo IIZUKA[1,2], Takanori MATSUMURA[1], Satoshi NAKAHIRA[3], Masaya HIGA[1], Masaru MATSUOKA[3,4], Mutsumi SUGIZAKI[3], Yoshihiro UEDA[5], Nobuyuki KAWAI[3,6], Mikio MORII[6], Motoko SERINO[3], Tatehiro MIHARA[3], Hiroshi TOMIDA[4], Shiro UENO[4], Hitoshi NEGORO[7], Arata DAIKYUJI[8], Ken EBISAWA[2], Satoshi EGUCHI[9], Kazuo HIROI[5], Masaki ISHIKAWA[10], Naoki ISOBE[11], Kazuyoshi KAWASAKI[4], Masashi KIMURA[12], Hiroki KITAYAMA[12], Mitsuhiro KOHAMA[4], Taro KOTANI[13], Yujin E. NAKAGAWA[3], Motoki NAKAJIMA[14], Hiroshi OZAWA[7], Megumi SHIDATSU[5], Tetsuya SOOTOME[3,15], Kousuke SUGIMORI[6], Fumitoshi SUWA[7], Hiroshi TSUNEMI[12], Ryuichi USUI[6], Takayuki YAMAMOTO[3,7], Kazutaka YAMAOKA[13], and Atsumasa YOSHIDA[3,13]

[1]Department of Physics, Faculty of Science and Engineering, Chuo University, 1-13-27 Kasuga, Bunkyo-ku, Tokyo 112-8551

[2]Institute of Space and Astronautical Science (ISAS), Japan Aerospace Exploration Agency (JAXA), 3-1-1 Yoshino-dai, Chuo-ku, Sagamihara, Kanagawa 252-5210

[3]MAXI team, RIKEN, 2-1 Hirosawa, Wako, Saitama 351-0198

[4]ISS Science Project Office, Institute of Space and Astronautical Science (ISAS), Japan Aerospace Exploration Agency (JAXA), 2-1-1 Sengen, Tsukuba, Ibaraki 305-8505

[5]Department of Astronomy, Kyoto University, Oiwake-cho, Sakyo-ku, Kyoto 606-8502

[6]Department of Physics, Tokyo Institute of Technology, 2-12-1 Ookayama, Meguro-ku, Tokyo 152-8551

[7]Department of Physics, Nihon University, 1-8-14 Kanda-Surugadai, Chiyoda-ku, Tokyo 101-8308

[8]Department of Applied Physics, University of Miyazaki, 1-1 Gakuen Kibanadai-nishi, Miyazaki, Miyazaki 889-2192

[9]National Astronomical Observatory of Japan, 2-21-1, Osawa, Mitaka City, Tokyo 181-8588

[10]School of Physical Science, Space and Astronautical Science, The graduate University for Advanced Studies (Sokendai), 3-1-1 Yoshino-dai, Chuo-ku, Sagamihara, Kanagawa 252-5210

[11]Institute of Space and Astronautical Science (ISAS), Japan Aerospace Exploration Agency (JAXA), 3-1-1 Yoshino-dai, Chuo-ku, Sagamihara, Kanagawa 252-5210

[12]Department of Earth and Space Science, Osaka University, 1-1 Machikaneyama, Toyonaka, Osaka 560-0043

[13]Department of Physics and Mathematics, Aoyama Gakuin University,5-10-1 Fuchinobe, Chuo-ku, Sagamihara, Kanagawa 252-5258

[14]School of Dentistry at Matsudo, Nihon University, 2-870-1 Sakaecho-nishi, Matsudo, Chiba 101-8308

[15]Department of Electronic Information Systems, Shibaura Institute of Technology, 307 Fukasaku, Minuma-ku, Saitama, Saitama 337-8570

*E-mail: tsuboi@phys.chuo-u.ac.jp

Received 2016 February 12; Accepted 2016 July 29

Abstract

23 giant flares from 13 active stars (eight RS CVn systems, one Algol system, three dMe stars and one YSO) were detected during the first two years of our all-sky X-ray monitoring with the gas propotional counters (GSC) of the Monitor of All-sky X-ray Image (MAXI). The observed parameters of all of these MAXI/GSC flares are found to be at the upper ends for stellar flares with the luminosity of 10^{31-34} ergs s^{-1} in the 2–20 keV band, the emission measure of 10^{54-57} cm^{-3}, the e-folding time of 1 hour to 1.5 days, and the total radiative energy released during the flare of 10^{34-39} ergs. Notably, the peak X-ray luminosity of $5^{+4}_{-2} \times 10^{33}$ ergs s^{-1} in the 2–20 keV band was detected in one of the flares on II Peg, which is one of the, or potentially the, largest ever observed in stellar flares. X-ray flares were detected from GT Mus, V841 Cen, SZ Psc, and TWA-7 for the first time in this survey. Whereas most of our detected sources are multiple-star systems, two of them are single stars (YZ CMi and TWA-7). Among the stellar sources within 100 pc distance, the MAXI/GSC sources have larger rotation velocities than the

other sources. This suggests that the rapid rotation velocity may play a key role in generating large flares. Combining the X-ray flare data of nearby stars and the sun, taken from literature and ou r own data, we discovered a universal correlation of $\tau \propto L_{\rm X}^{0.2}$ for the flare duration τ and the intrinsic X-ray luminosity $L_{\rm X}$ in the 0.1–100 keV band, which holds for 5 and 12 orders of magnitude in τ and $L_{\rm X}$, respectively. The MAXI/GSC sample is located at the highest ends on the correlation.

Key words: stars: flare - stars: activity - stars: late-type - stars: variables general - stars: rotation

1 Introduction

Cool stars, which have spectral types of F, G, K, and M, are known to show X-ray flares. The flares are characterized with the fast-rise and slow-decay light curve. The flares generally accompany the rise and decay in the plasma temperature. The general understanding, based on the numerous studies of solar flares, is that such features arise as a consequence of a sudden energy release and relaxation process in the reconnection of magnetic fields on/around stellar surfaces. In solar flares, the reconnection, which occurred in somewhere at large coronal heights, accelerates primarily electrons (and possibly ions) up to MeV energies, and the electrons precipitate along the magnetic fields into the chromosphere, suddenly heating the plasma at the bottom of the magnetic loop to very high temperatures. A large amount of plasma streams from the bottom to the top of the magnetic loop, while cooling has already started by that time. The flare temperature thus peaks before the Emission Measure (*EM*) does, or analogously, harder emission peaks before softer emission.

Numerous studies on flare stars have been made with pointing observations. For the reviews, see Pettersen (1989), Haisch et al. (1991), Favata & Micela (2003), Güdel (2004), and references therein. However, we cannot yet answer some fundamental questions, such as how large a flare a star can have, and how very large flares are generated. The poor understanding is rooted in the fact that the larger flares occur less frequently. Hence, all-sky monitoring is crucial to detect such large flares.

X-ray all-sky monitors like Ariel-V/SSI, GRANAT/WATCH, and Swift/BAT have detected some large stellar flares. Using the data of Ariel-V/SSI spanning for 5.5 years, Pye & McHardy (1983) and Rao & Vahia (1987) detected in total twenty flares from seventeen stellar sources, including ten RS CVn systems and seven dMe stars. Rao & Vahia (1987) showed that there is a positive correlation between the bolometric luminosity and the X-ray peak luminosity. GRANAT/WATCH detected two X-ray transients, which have a counterpart of a flare star in their respective positional error boxes

(Castro-Tirado et al. 1999). Swift with BAT prompted the follow-up observations with XRT after detecting large flares from an RS CVn system II Peg (Osten et al. 2007) and that from a dMe star EV Lac (Osten et al. 2010). Flares from two other RS CVn stars (CF Tuc and UX Ari) have been detected with Swift/BAT (Krimm et al. 2013).

Following successful detections of large flares with all-sky X-ray surveys, we executed a survey of stellar flares with the Monitor of All-sky X-ray Image (MAXI; Matsuoka et al. 2009). MAXI is a mission of an all-sky X-ray monitor operated in the Japanese Experiment Module (JEM; Kibo) on the International Space Station (ISS) since 2009 August. It observes an area in the sky once per 92 min orbital cycle, and enables us to search for stellar flares effectively. In this paper, we report the results with the gas proportional counters (GSC) of MAXI obtained by the first two-years operation from 2009 August to 2011 August. The results with the CCD camera of MAXI (SSC) will be given elsewhere. We describe the MAXI observation in §2, our flare-search method and the results in §3, then discuss the properties of the detected flares and the flare sources in §4.

2 Observations

The MAXI has two types of slit cameras, the GSC and SSC, both of which incorporate X-ray detectors consisting of gas proportional counters and X-ray CCDs, respectively. These detectors cover an energy range of 2 to 30 keV and 0.5 to 12 keV, respectively (Matsuoka et al. 2009; Tsunemi et al. 2010; Tomida et al. 2011; Mihara et al. 2011). As stated in section §1, the observations of stellar flares examined here were conducted by the GSC, which has a larger field of view (FoV) and then sky coverage than SSC. The GSC achieves better sensitivity in the 2–10 keV band than any other X-ray all-sky monitors so far using large-area proportional counters with a low background, and then is preferable to detect stellar flares. The data from 2009 August 15th to 2011 August 15th are used here.

The GSC consists of twelve pieces of proportional counters, which employ resistive carbon-wire anodes to acquire one-dimensional position sensitivity. Each set of two counters forms a single camera unit, of which the GSC has six in total. The overall FoV is a slit shape of $160^\circ \times 3^\circ$ in the horizon and zenith directions, respectively, which allows the MAXI to scan the entire sky twice as the ISS moves; i.e., MAXI/GSC can scan 97% of the entire sky with each ISS orbit. When the ISS passes high background regions such as the South Atlantic Anomaly, the high voltage of the GSC is switched off to protect the proportional counters from damage. Then, the actual sky coverage is about 85% of the whole sky per 92-minute orbital period, 95% per day, and 100% per week.

The point spread function (PSF) in the Anode-Wire Direction is determined by the angular re-

sponse of the slit-and-slat collimator and the positional response of the position-sensitive gas counter along the anode wire. The collimator is designed to have an angular resolution of $1.^{\circ}0$–$1.^{\circ}5$ in FWHM, depending on the X-ray incident angle in the Anode-Wire Direction and X-ray energy. The PSF in the scan direction is determined with the modulated time variations of the detector area, which changes according to the triangular transmission function of the collimator during each transit. The GSC typically scans a point source on the sky during a transit of 40–150 seconds with a FoV of $1.^{\circ}5$-width (FWHM) every 92-minute orbital period. The transit time depends on the source incident angle in the Anode-Wire Direction. The detector area for the target changes according to the triangular transmission function of the collimator during each transit. The peak value is 4–5 cm^2 per one camera. The detailed performance of the GSC was described by Sugizaki et al. (2011). All the data we used were delivered from the MAXI database system (Negoro et al. 2016).

3 Analysis and Results

3.1 Search for Flaring Stars

In order to search for flares from stars, we used the alert system "nova search" (Negoro et al. 2010). The alert system on the ground swiftly reports X-ray transient events to astronomers worldwide, prompting potential follow-up observations. For a further search, we have created movies of GSC image for each sky area segmented into circles of 10° radii, setting the observation time of one day for one shot. The entire sky is covered with about 200 segments.

From the confirmed transient events, we selected events whose peaks are located within 2° from nearby known stellar sources. The source lists are composed of the catalogs of Torres et al. (2006), López-Santiago et al. (2006), and Riedel et al. (2014). The locations of the X-ray peaks are determined automatically for the sources confirmed by "nova search", or by eye from the movies for the others. For these selected stellar-flare candidates, we proceeded to the following identification process.

3.2 Significance in Source Detection

We estimated the significance of a detected source with the same method employed in Uzawa et al. (2011), as follows: (1) extracting events within a circle with $1.^{\circ}5$ radius centered at the transient event ("source region") in the 2–10 keV band, (2) $\sim$10 circle regions, whose radii are all $1.^{\circ}5$, are chosen around the source region ("background circles"), (3) counting the numbers of events in the 2–10 keV band in each background circle, (4) the average of the counts in a background circle is defined as the background level, (5) the standard deviation of the counts in a background circle is regarded as the

1-σ background fluctuation, (6) subtracting the background level from the counts in the source region, and the residual is regarded as the source counts, (7) the source counts divided by the 1-σ background fluctuation is defined as the source significance.

In the first flare on II Peg (FN15 in table 1) on 2009 August 20th, the source was in a high-noise area, located close to the wire edge. Thus, we set the background circles in the high-noise area in order to estimate the appropriate level of the background. The time-spans, for which we extracted the data, are indicated in the light curves with horizontal bars in figure 1.

3.3 Reconfirmation of the Source Positions

The number of the stellar flare candidates with the significance larger than 5-σ level were twenty-three in total. For these flares, we further performed two-dimensional image fittings to obtain the precise error regions for the X-ray positions. The fitting algorithm is given in Morii et al. (2010). The shape of the region can be approximated with an ellipse with the typical semi-major and semi-minor axes of $0\overset{\circ}{.}7$ and $0\overset{\circ}{.}5$, respectively, at 90% confidence level. We found that all the error regions still encompass the position of each stellar counterpart in our list, which we had seen within 2° from the X-ray peak. We also confirmed that all the stellar counterparts are listed in the ROSAT bright source catalog (Voges et al. 1999). No other ROSAT bright-sources are in the same error regions for all the events but one; the error region of FN20 (see table 1) encompasses AT Mic (1RXS J204151.2$-$322604) and 1RXS J204257.5$-$320320. 1RXS J204257.5$-$320320 is not in our list of nearby sources, and the detailed nature is not known. Moreover, certainly no X-ray variation has ever been reported. Then we regard that the transient occurred on the established flare star, AT Mic. The dates of each flare, the error regions, the X-ray counts rates, the significant levels, and the stellar counterparts are summarized in table 1.

The detected twenty-three flares were found to come from thirteen stars; eight RS CVn systems (VY Ari, UX Ari, HR1099, GT Mus, V841 Cen, AR Lac, SZ Psc and II Peg), one Algol-type star (Algol), three dMe stars (AT Mic, EQ Peg and YZ CMi), and one YSO (TWA-7). Note that the detection of the flare from TWA-7 has been already reported in Uzawa et al. (2011). We list the fundamental parameters of the stellar counterparts in table 2. Four out of thirteen sources showed flares multiple times. We adopt the source distances listed in table 2 when we estimate or discuss the physical parameters in this paper. The distances are all within 100 pc, except that of GT Mus (172 pc). Figure 2 displays the relation between the source distance and $L_{\rm X}$. This implies that our detection limit is roughly 10 mCrab in the 2–20 keV band.

3.4 Timing Analysis

Figure 1 shows the GSC light-curves of all the detected flares in the 2–10 keV band. In making the light-curves, the data for the sources were extracted from the circles with the radii ranging from $1.^\circ3$ to $1.^\circ7$, which are selected depending on the signal-to-noise ratio. The backgrounds are extracted from the annuli with the inner and outer radii of 2° and 4°, respectively, except for the following two cases, in which an edge of a wire is close to the source region. In the case of the flare on HR1099 (FN5) on 2010 January 23th, we chose the background region as an annulus with the inner and outer radii of 2° and $3.^\circ5$, respectively, to eliminate a high-noise area. As for the first flare on II Peg (FN15) on 2009 August 20th, since the source was more closely located to a wire edge than the HR1099 case, the source region was just in the high-noise area. Thus, in order to remove the appropriate level of the background, we chose the background region as a rectangle of $3.^\circ4 \times 19^\circ$, removing a central circle with $1.^\circ7$ radius. After subtracting the background, all the extracted source-counts were normalized by dividing by the total exposure (in units of cm^2 s), which is obtained with a time integral of the collimator effective area. We fitted them with a burst model, which is described as a linear rise followed by an exponential decay. The e-folding times are shown in table 3 and figure 3, which range from about 1 hour (AR Lac) to 1.5 days (GT Mus).

3.5 Spectral Analysis

We also analyzed X-ray spectra in flare phases. The GSC spectra were extracted during the time interval indicated with the horizontal bars on the light-curves (figure 1), as those used in the estimation of the significance of source detection. We used the same source and the background regions as those used in the timing analysis. Since the photon-statistics are limited, we fitted the spectra with a simple model; a thin-thermal plasma model (*mekal*: Mewe et al. 1985; Mewe et al. 1986; Kaastra 1992; Liedahl et al. 1995) with the fixed abundance ratios of heavy elements to the solar values. We ignored the interstellar absorption, since all the sources are located within 200 pc and are not in famous molecular clouds. An example of a spectrum with the best-fit model is found in the figure 2 in Uzawa et al. (2011). Table 3 and figure 3 give the best-fit parameters and the distribution of the derived properties (*EM*, $L_{\rm X}$, e-folding time, the total energy), respectively[1].

[1] One might guess that significantly different results may be obtained with different plasma models, such as *apec* (Smith et al. 2001). Then, we fitted the spectra of FN5, FN9 and FN16 with the *apec* model and found that the obtained parameters (kT, EM, $L_{\rm X}$) were consistent with each other between the *mekal* and *apec* models for a wide range of temperature.

4 Discussion

4.1 Detected Flares and the Source Categories

We detected twenty-three flares, whose X-ray luminosities are 10^{31-34} ergs s^{-1} in the 2–20 keV band and the emission measures are 10^{54-57} cm^{-3}. The flares released the energy of 10^{34-39} ergs radiatively with the e-folding times of 1 hour to 1.5 days (see figure 3). All the detected flares are from active stars; eight RS CVn systems, one Algol system, three dMe stars and one YSO, totaling thirteen stars. This confirms that RS CVn systems and dMe stars are intense flare sources, as reported in Pye & McHardy (1983) and Rao & Vahia (1987). The X-ray flares from GT Mus, V841 Cen, SZ Psc, and TWA-7 were detected for the first time in this survey. Notably, II Peg showed the $L_{\rm X}$ of $5^{+4}_{-2} \times 10^{33}$ ergs s^{-1} in the 2–20 keV band at the peak of the flare, which is one of the largest ever observed in the stellar flares.

Most of the flare sources that we detected with MAXI/GSC are multiple-star system (see table 2). However, two of them were single stars: TWA-7 (Uzawa et al. 2011) and YZ CMi. In addition, another two (AT Mic and EQ Peg) have, though a binary system, a very wide binary-separation of roughly 6000 $R_\odot$, and so are the same as single stars practically. All of these four stars are known to have no accretion disk. These results reinforce the scenario that neither binarity (e.g. Getman et al. 2011) nor accretion (e.g. Kastner et al. 2002, Argiroffi et al. 2011), nor star-disk interaction (e.g. Hayashi et al. 1996, Shu et al. 1997, Montmerle et al. 2000) is essential to generate large flares, as has been already discussed in Uzawa et al. (2011).

According to the catalog of active binary stars (Eker et al. 2008), 256 active binaries (e.g. RS CVn binaries, dMe binaries etc.) are known within the distance of 100 pc from the solar system. However, we detected flares from only ten of them. Four of them (UX Ari, HR1099, AR Lac and II Peg) exhibited flares more than twice.

4.2 X-ray Activity on Solar-type Stars

As for the solar-type stars, fifteen G-type main-sequence stars are known within the 10-pc distance (from *AFGK "bright" stars within 10 parsecs*[2]). The MAXI/GSC has not detected any X-ray flares from these stars. The nearest G-type star is α Cen A (G2 V) at the distance of 1.3 pc (Söderhjelm 1999). The upper limit on the $L_{\rm X}$ of α Cen A is estimated to be 2×10^{28} ergs s^{-1}, based on the detection limit of 10 mCrab with MAXI/GSC. This is consistent with the X-ray luminosities observed in solar flares; $L_{\rm X}$ is mostly lower than 10^{27}–10^{28} ergs s^{-1} (Feldman et al. 1995). However, large X-ray flares with the respective $L_{\rm X}$ of 10^{29} ergs s^{-1} and 2×10^{31} ergs s^{-1} have been observed

[2] http://www.solstation.com/stars/pc10afgk.htm#yellow-orange

from ordinary solar-type stars π^1 UMa (Landini et al. 1986) and BD+10°2783 (Schaefer et al. 2000). Schaefer et al. (2000) called such flares "superflares". So far, very few extensive studies have been made in the X-ray band and reported to give any good constraints on the frequency of the occurrence of "superflares" in the band. Our MAXI/GSC two-year survey is the best X-ray study of this kind. From our result, we can claim that the flares with $L_{\rm X}$ of larger than 1×10^{30} ergs s^{-1} must be very rare for solar-type stars.

4.3 EM vs. kT and the Derived Loop Parameters

Figure 4 shows a plot of EM vs. plasma temperature (kT) for the flares in our study of the MAXI/GSC sources, together with solar flares (Feldman et al. 1995), solar microflares (Shimizu 1995), and flares from the stars in literature (see table 4 for the complete set of references). All of the plotted samples are roughly on the universal correlation over orders of magnitude (Feldman et al. 1995, Shibata & Yokoyama 1999). Our sample is located at the high ends in the correlation for both the temperatures and emission measures.

Now, we consider the two important physical parameters of flares, that is, the size and magnetic field. Shibata & Yokoyama (1999) formulated the theoretical EM-kT relations for a given set of a loop-length and magnetic field as equations (5) and (6) in their paper[3] (see figure 4 for a few representative cases). We calculated the loop-length and magnetic-field strength for each of the observed flares with MAXI-GSC, based on the relations (Shibata & Yokoyama 1999), as listed in table 3. The magnetic field of our sample is comparable with those of flares on the Sun ($\sim$15–150 G). On the other hand, our sample has orders of magnitude larger sizes of flare loops than those on the Sun ($<$0.1 $R_\odot$). Especially noteworthy ones among our sample are the two largest flares relative to their binary separations, FN4 from UX Ari and FN16 from II Peg. Their loop lengths are 10 and 20 times larger than their respective binary separations, which are unprecedentedly large among stellar flares.

The extraordinary large loop lengths could possibly be an artifact due to the systematic error in the model by Shibata & Yokoyama (1999). In fact, their derived loop lengths are 10 times larger than those obtained by Favata et al. (2001), who used a hydrodynamic model by Reale & Micela (1998). In Shibata & Yokoyama (2002), which is the follow-up paper of Shibata & Yokoyama (1999), it is argued that their derived loop length could be reduced to roughly 1/10 if the two assumptions (the

[3] Their calculation of the EM-kT relations is based on the magnetohydrodynamic numerical simulations of the reconnection by Yokoyama & Shibata (1998). The simulation takes account of heat conduction and chromospheric evaporation on the following four assumptions: (1) the plasma volume is equal to the cube of the loop length, (2) the gas pressure of the confined plasma in the loop is equal to the magnetic pressure of the reconnected loop, (3) the observed temperature at the flare peak is one-third of the maximum temperature at the flare onset, (4) the pre-flare proton (= electron) number density outside the flare loop is 10^9 cm^{-3}.

points 3 and 4 mentioned in the footnote below) are altered. In our MAXI sample, even if the true loop sizes are 1/10 of the above-estimated values as a conservative case, the largest ones are 0.2–5 times larger than their binary separation and so are still large.

4.4 Duration vs. X-ray Luminosity

We search for potential correlations in various plots to study what are the deciding factors to generate large stellar flares and to which extent. Figure 5 plots the duration of flares ($\tau_{\rm lc}$) vs. the intrinsic X-ray luminosity ($L_{\rm X_bol}$) in the 0.1–100 keV band for the stars detected with MAXI/GSC and with other missions (see table 4 for the complete set of references). Here, we have introduced $L_{\rm X_bol}$ in order to take all the radiative energy into our calculation [4]. Solar flares (Pallavicini et al. 1977, Shimizu 1995, Veronig et al. 2002) too are superposed [5]. The data points of the MAXI/GSC flares are found to be located at the highest ends in both the $L_{\rm X_bol}$ and duration axes among all the stellar flares. The plot indicates that there is a universal correlation between $L_{\rm X_bol}$ of a flare and its duration, such that a longer duration means a higher $L_{\rm X_bol}$. Remarkably, the correlation holds for wide ranges of parameter values for $10^{22} \lesssim L_{\rm X_bol} \lesssim 10^{34}$ ergs s^{-1} and $10^{1} \lesssim \tau_{\rm lc} \lesssim 10^{6}$ s. Using the datasets of the stellar flares detected with MAXI (this work) and other missions (table 4), and the solar flares reported by Pallavicini et al. (1977), we fitted the data with a linear function in the log-log plot [6] and obtained the best-fit function of

$$\tau_{\rm lc} = (1.1^{+4.7}_{-0.9}) \times 10^{4} \left(\frac{L_{\rm X_bol}}{10^{33}\ {\rm ergs\ s^{-1}}} \right)^{0.20 \pm 0.03} {\rm sec}, \quad (1)$$

where the errors of both the coefficient and the power are in 1-σ confidence level. The best-fit model is shown with a solid line in figure 5 top panel. We found that the best-fit model agrees also with the range of the data for solar microflares reported by Shimizu (1995), even though the luminosities $L_{\rm X_bol}$ of their data are smaller than $\sim 10^{25}$ ergs s^{-1}, whereas those used for our fitting are larger than that.

For comparison, Veronig et al. (2002) and Christe et al. (2008) have derived similar power-law slope as ours, $\sim$0.33 for the GOES data and $\sim$0.2 for the RESSI data, respectively, though with the

[4] See Appendix for the detailed process to derive $L_{\rm X_bol}$ for each data-set.

[5] As the duration, we used e-folding time for each flare in our work and the works introduced in table 4. For the data of Pallavicini et al. (1977) and that of Veronig et al. (2002), we used "decay time", of which the definitions are up to the corresponding authors. For the data of Shimizu (1995), we used the duration itself in FWHM reported in the paper. Generally, flares in any magnitude have fast-rise and slow-decay light curves, and the rise times at longest are comparable to the corresponding decay times (e.g. Pallavicini et al. 1977, Imanishi et al. 2003). Therefore the samples are consistent with one another within a factor of 2, or 0.3 in the logarithmic scale as in the vertical axis of figure 5.

[6] Shimizu (1995) and Veronig et al. (2002) presented the plots which indicate the X-ray luminosity and duration of each flare, but not tables for them to give the exact values. Then we excluded both datasets from the fitting.

limited energy bands. The ranges of their luminosities are $L_{\rm X} = 10^{23.5-25.5}$ ergs s^{-1} in the 3.1–24.8 keV band and $L_{\rm X} = 10^{22.5-25.5}$ ergs s^{-1} in the 6–12 keV band, respectively.

In the following subsections, we discuss the plausible models to explain this positive correlation, examining three potentially viable scenarios: the radiative-cooling dominant, conductive-cooling dominant, and propagating-flare models. Note that we have chosen the former two models for simplicity and examine them separately, although it is expected, as most star-flare models assume, that both radiation and conduction are present in a flare and that the latter is active early in the decay and the former is, later (e.g. Shibata & Yokoyama 2002, Cargill 2004, Reale 2007). We assume that the duration of a flare $\tau_{\rm lc}$ represents the cooling time of the heated plasma when we examine the radiative- and conductive-cooling dominant models.

4.4.1 Radiative Cooling Model

First, we consider the condition where the radiative cooling is dominant. Since the thermal energy is lost via radiation, $\tau_{\rm lc}$ and the radiative cooling time $\tau_{\rm rad}$ are given by,

$$\tau_{\rm lc} \simeq \tau_{\rm rad} = \frac{3 n_{\rm e} k T}{n_{\rm e}^2\, F(T)} = \frac{3 k T}{n_{\rm e}\, F(T)}, \tag{2}$$

where $n_{\rm e}$ and $F(T)$ are the electron density and radiative loss rate, respectively. We obtained the radiative loss rate, using the *CHIANTI* atomic database (version 8.0) and the *ChiantiPy* package (version 0.6.4) [7].

On the other hand, based on the plot of EM vs. kT (figure 4), we confirm that most of the observed data of stellar and solar flares are confined in the region of 15 G $< B <$ 150 G, where B is magnetic field strength. The region is mathematically described as

$$EM \simeq 10^{48}\, \alpha^{-5} \left(\frac{T}{10^7\ {\rm K}} \right)^{17/2}\ {\rm cm}^{-3}\ , \tag{3}$$

where α is a non-dimensional parameter ranging between 0.3 and 3. Since the derived EM and $F(T)$ compose $L_{\rm X_bol}$ as

$$L_{\rm X_bol} = EM\ F(T)\ , \tag{4}$$

we obtain, combining it with equation (3),

$$L_{\rm X_bol} \simeq 10^{48}\, \alpha^{-5} \left(\frac{T}{10^7\ {\rm K}} \right)^{17/2}\ F(T)\ . \tag{5}$$

Now that both $\tau_{\rm lc}$ and $L_{\rm X_bol}$ have been parameterized with the temperature T, we insert solid lines in figure 5 as their relation for radiative-cooling dominant model.

[7] http://www.chiantidatabase.org/chianti.html

Observationally, the electron density $n_{\rm e}$ was measured to be 10^{11} cm^{-3} in flares of Proxima Centauri with a high-resolution spectroscopy in the X-ray band (Güdel et al. 2002). In the solar flares, $n_{\rm e}$ of 10^{10-11} cm^{-3} has been calculated from the EM and the volume of the loop (Pallavicini et al. 1977). Some other spectroscopic observations of solar flares have indicated a wide range of $n_{\rm e}$; 10^{11-13} cm^{-3} (see references in Güdel 2004). Therefore, we derived the permitted ranges for radiative cooling plasma in the following two cases: (1) $n_{\rm e} = 10^{11}$ cm^{-3} and α= 0.3–3 (figure 5 middle panel), (2) $n_{\rm e} = 10^{10-13}$ cm^{-3} and α = 1 (figure 5 bottom panel). With the wide permitted range, the figures indicate that radiative cooling explains all the flares in our dataset.

4.4.2 Conductive Cooling Model

Second, we consider the condition where the conductive cooling is dominant, assuming a semicircular loop of the flare with the cross-section of $\pi \left(\frac{l}{10}\right)^2$ for the half-length l, which is often observed in solar flares. In this case, $\tau_{\rm lc}$ and the conductive cooling time $\tau_{\rm con}$ are given by

$$\begin{aligned}\tau_{\rm lc} \simeq \tau_{\rm con} &= \frac{3 n_{\rm e} k T}{10^{-6}\ T^{7/2}\ l^{-2}} \\ &= 1.3 \times 10^2 \left(\frac{n_{\rm e}}{10^{11}\ {\rm cm}^{-3}}\right) \\ &\times \left(\frac{T}{10^7\ {\rm K}}\right)^{-5/2} \left(\frac{l}{10^9\ {\rm cm}}\right)^2 {\rm sec}. \end{aligned} \tag{6}$$

On the other hand, a fraction of the thermal energy is observed as radiation. The luminosity $L_{\rm X_bol}$ and EM for the temperature T are written as equations (4) and (3), respectively. With the plasma volume of $\frac{\pi}{50} l^3$, EM is also written as,

$$EM = \frac{\pi}{50}\ n_{\rm e}^2\ l^3\ . \tag{7}$$

Combining equations (3), (6) and (7) gives

$$\tau_{\rm lc} \simeq 1.3 \times 10^5 \left(\frac{50}{\pi}\right)^{2/3}\ \alpha^{-10/3}\ n_{\rm e}^{-1/3}\ \left(\frac{T}{10^7\ {\rm K}}\right)^{19/6}\ . \tag{8}$$

Now that both $\tau_{\rm lc}$ and $L_{\rm X_bol}$ have been parameterized with the temperature T, we insert dotted lines in figure 5 as their relation for conductive-cooling dominant model. The values of $n_{\rm e}$ and α are varied independently within the ranges of $10^{10} \lesssim n_{\rm e} \lesssim 10^{13}$ cm^{-3} and $0.3 \lesssim \alpha \lesssim 3$, respectively. The figure indicates that the model and the data overlap with each other in the given parameter space.

4.4.3 Propagating Flare Model

Third, we examine spatially propagating flare, like two-ribbon flares seen on the Sun. The total energy released during a flare via radiation, $E_{\rm rad}$, is described as

$$E_{\rm rad} \simeq \tau_{\rm lc} L_{\rm X_bol}\ . \tag{9}$$

On the other hand, $E_{\rm rad}$ originates from thermal energy confined in the plasma, and the thermal energy comes from stored magnetic energy, $E_{\rm mag}$. Then, it can be also written as

$$E_{\rm rad} = f\ E_{\rm mag} = \frac{f\ B^2\ D^3}{8\pi}\ , \tag{10}$$

where f is the energy conversion efficiency from magnetic energy to that released as radiation, and D is the scale length of the flaring region. When we assume that the magnetic reconnection propagates with the speed v, $\tau_{\rm lc}$ satisfies the following formula

$$\tau_{\rm lc} = D/v\ . \tag{11}$$

Eliminating $E_{\rm rad}$ and D with the equations (9), (10) and (11), we obtain

$$\tau_{\rm lc} \simeq 1.2 \times 10^4 \left(\frac{f}{0.1}\right)^{1/2} \left(\frac{B}{50\ {\rm G}}\right)^{-1} \times \left(\frac{v}{3 \times 10^7\ {\rm cm\ s^{-1}}}\right)^{-3/2} \left(\frac{L_{\rm X_bol}}{10^{33}\ {\rm ergs\ s^{-1}}}\right)^{1/2} {\rm sec}. \tag{12}$$

If the values of f, B and v are common among stars,

$$\tau_{\rm lc} \propto L_{\rm X_bol}^{1/2}\ . \tag{13}$$

The power of $L_{\rm X_bol}$ is slightly larger than what we obtained.

4.5 Origin of Large Flares

4.5.1 Rotation Velocity

The positive correlation between quiescent X-ray luminosity and rotation velocity has been reported by Pallavicini (1989) and in subsequent studies. However, no studies have been published about this type of correlation for the flare luminosity. Compiling our data sample and those in literature, we search for the potential correlation of this kind.

We plot the total energy released during a flare (i.e., $E_{\rm rad}$) vs. the square of rotation velocity ($v_{\rm rot}^2$) in figure 6, where $E_{\rm rad}$ is derived by multiplying $L_{\rm X}$ in the 2–20 keV band by the e-folding time of the flare decaying phase[8]. From figure 6, we find that the MAXI sample is concentrated at the region of the high rotation velocity and the large total energy. This is the first indication with an unbiased survey that stellar sources with higher rotation velocities can have a very high $E_{\rm rad}$.

In order to validate this tendency further, we made two histograms of the number of sources as a function of the star-rotation velocity for flare sources. One is for our MAXI/GSC sample, and the

[8] If flares have been detected from a source multiple times with MAXI and/or other missions, only the largest total energy is used. If the flare source is a multiple-star system, we use the rotation velocity of the star with the largest stellar radius in the system. In our sample, the source with the largest radius has a higher velocity than the other stars in the same system for all the multiple-star systems except EQ Peg.

other is for cataloged nearby stars from the literature (active binaries; Eker et al. 2008, X-ray-detected stellar sources; Wright et al. 2011). Both the samples are within 100 pc distance, and from the latter sample, MAXI/GSC sources are excluded. Figure 7 shows the two histograms. The MAXI/GSC sources have the median logarithmic rotation velocity of 1.52 in units of log (km s^{-1}) with the standard deviation of 0.37 dex. On the other hand, the undetected sources with MAXI/GSC have the median logarithmic value of 0.80 in the same units with the standard deviation of 0.52 dex. Therefore, the rotation velocities of the MAXI sources, which have shown huge flares as reported in this paper, are significantly higher than those of the other active stars that are comparatively quiet. This supports that the sources with faster velocities generate larger flares.

4.5.2 Stellar Radius

We investigate whether the MAXI sources and/or the size of the flare-emitting region have any common characteristics or correlations in their stellar radii.

Figure 8 plots EM vs. the square of the stellar radius (R_*^2) for the stars detected with MAXI/GSC and those detected with other missions (see table 4 for the complete set of references)[9]. Though the sample is limited, a hint of the positive correlation between EM and R_*^2 is seen at least in the MAXI/GSC sources[10].

We also made a number-distribution histogram as a function of the radius in figure 9, similar to figure 7. From figure 9, we find MAXI/GSC sources are concentrated at the radii of about 3 and 0.3 $R_\odot$, which correspond to RS CVn-type and dMe stars, respectively. On the other hand, the undetected sources with MAXI/GSC are widely distributed in figure 9, which implies that the magnitude of flares is not as sensitive to the stellar radius as to the rotation velocity.

5 Summary

1. During the two-year MAXI/GSC survey, we detected twenty-three energetic flares from thirteen active stars (eight RS-CVn stars, three dMe stars, one YSO, and one Algol type star). The physical parameters of the flares are very large for stellar flares in all of the followings: the X-ray luminosity $L_{\rm X}$ (10^{31-34} ergs s^{-1} in the 2–20 keV band), the emission measure EM (10^{54-57} cm^{-3}), the e-folding time (10^{3-6} s), and the total energy released during the flare (10^{34-39} ergs).
2. The flares from GT Mus, V841 Cen, SZ Psc and TWA-7 were detected for the first time in the

[9] The largest EM is used for each source if flares have been detected multiple times, and the radius of the larger star is used if the source is a multiple-star system.

[10] A similar plot has been made by Rao & Vahia (1987), for the flares detected with Ariel-V/SSI, which shows a similar correlation to ours, although their plot was the bolometric luminosity vs. X-ray peak luminosity.

X-ray band. From II Peg, we detected one of the largest flares among stellar flares with $L_{\rm X}$ of $5^{+4}_{-2} \times 10^{33}$ ergs s^{-1} in the 2–20 keV band. Whereas most of the sources detected with MAXI/GSC are multiple-star systems, two of them (YZ CMi and TWA-7) are single, which are known to have no accretion disk. These results reinforce the scenario that none of binarity, accretion, and star-disk interaction is essential to generate large flares, as has been already discussed in Uzawa et al. (2011).

3. The survey showed that the number of the sources that show extremely large flares is very limited; only ten out of the 256 active binaries within the 100 pc distance have been detected, while four of the ten sources showed flares multiple times. We detected no X-ray flares from solar-type stars, despite the fact that fifteen G-type main-sequence stars lie within 10-pc distance. This implies that the frequency of the superflares from solar-type stars, which has $L_{\rm X}$ of more than 1×10^{30} ergs s^{-1}, is very small.
4. On the EM–kT plot, our sample is located at the high ends in the universal correlation, which ranges over orders of magnitude (Feldman et al. 1995, Shibata & Yokoyama 1999). According to the theory of Shibata & Yokoyama (1999), our sample has the similar intensity of magnetic field to those detected on the Sun ($\sim$15–150 G), but has orders of magnitude larger flare-loop sizes than those on the Sun ($< 0.1\ R_\odot$). The largest two loop sizes from UX Ari and II Peg are huge, and are much larger than the binary separations.
5. We plotted the duration vs $L_{\rm X_bol}$, using the data of solar and stellar flares in literature and the data of the flares on MAXI/GSC sources. The plot indicates that there is a universal positive correlation between $L_{\rm X_bol}$ of a flare and its duration, such that a longer duration means a higher $L_{\rm X_bol}$. The correlation holds for the wide range of parameter values; 12 and 5 orders of magnitude in $L_{\rm X_bol}$ and duration, respectively. Our sample is located at the highest ends on the correlation. From the data, we found that the duration is proportional to $L^{0.2}_{\rm X_bol}$.
6. Our sample has especially fast rotation velocities with an order of 10 km s^{-1}. This indicates that the rotation velocity is an essential parameter to generate big flares.

We thank M. Sakano, Y. Maeda, F. Reale, and S. Takasao for useful discussion. This research has made use of the MAXI data[11], provided by the RIKEN, JAXA, and MAXI teams. This research was partially supported by the Ministry of Education, Culture, Sports, Science and Technology (MEXT), Grant-in-Aid No.19047001, 20041008, 20244015, 20540230, 20540237, 21340043, 21740140, 22740120, 23540269, 16K17667, and Global-COE from MEXT "The Next Generation of Physics, Spun from Universality and Emergence" and "Nanoscience and Quantum

[11]http://maxi.riken.jp/top/index.php

Physics". Y.T. acknowledges financial support by a Chuo University Grant for Special Research.

Appendix. The process to derive $L_{\rm X_bol}$ for each dataset

In §4.4, we derived the intrinsic X-ray luminosity $L_{\rm X_bol}$ in the 0.1–100 keV band from the available observed X-ray data in narrower energy bands (Pallavicini et al. 1977, Shimizu 1995, Veronig et al. 2002). The process to derive it is as follows.

1. In principle, we derive $L_{\rm X_bol}$ from the parameters kT and EM, using the equation 4. As for the X-ray data of Shimizu (1995) and Veronig et al. (2002), it is necessary to estimate the values of kT and EM from the X-ray luminosities in the GOES band (3.1–24.8 keV) (hereafter $L_{\rm X_GOES}$). To estimate them, first, we derive the ratios (denoted as $P(T)$) of the X-ray luminosity in the GOES band to that in the 0.1–100 keV band (i.e., $L_{\rm X_bol}$) as a function of kT, using the $apec$ model in $XSPEC$. Next, assuming the empirical relation of EM vs.kT for flares, (equation 3), we obtain EM as a function of kT, with the parameter α fixed to one (hereafter $EM(T)$). Combining these parameters with equation 4, the GOES band luminosity is written as
$$L_{\rm X_GOES} = L_{\rm X_bol}\ P(T) = F(T)\ EM(T)\ P(T). \quad \text{(A1)}$$
We can derive T for each $L_{\rm X_GOES}$, and then obtain $L_{\rm X_bol}$ with this formula.
2. As for the X-ray data of Pallavicini et al. (1990a), we simply accept the X-ray luminosities in the 0.05–2 keV band in their paper as $L_{\rm X_bol}$, because the luminosities in the band are estimated to be about 95% of $L_{\rm X_bol}$. Note that we have used the $apec$ model in $XSPEC$, varying the temperatures in the range of log T = 6.5–7.3 (K), to get the ratio of 95%, where the range for the temperatures is assumed by Pallavicini et al. (1990a).

Table 1. Date and other observed parameters of each flare.

Flare	MJD*	UT*	Error Ellipse				Count Rate†	Significance	Counterpart	Category
			Center(J2000)	Semimajor axis	Seminor axis	Roll angle				
		[YYYY MMM DD HH:MM:SS]	[HH:MM:SS, DDD:MM:SS]	[degree]	[degree]	[degree]	[10^{-2}counts s^{-1}]	[σ]		
FN1	55144.347	2009 Nov 09 08:19:15	02:49:55.49, +31:18:32.34	1.0	0.82	90	1.1	7.4	VY Ari	RS CVn
FN2	55080.193	2009 Sep 06 04:37:45	03:26:33.38, +28:31:36.03	0.6	0.57	90	0.72	9.5	UX Ari	RS CVn
FN3	55662.965	2011 Apr 11 23:09:50	03:26:06.13, +28:49:51.75	0.31	0.26	0	12	14	UX Ari	RS CVn
FN4	55678.049	2011 Apr 27 01:10:25	03:26:09.44, +28:47:41.58	0.44	0.36	110	32	16	UX Ari	RS CVn
FN5	55219.221	2010 Jan 23 05:18:10	03:37:02.86, +00:42:24.30	0.5	0.43	170	17	24	HR1099	RS CVn
FN6	55244.054	2010 Feb 17 01:17:51	03:36:28.02, +00:23:58.80	0.43	0.39	90	0.53	7.1	HR1099	RS CVn
FN7	55503.647	2010 Nov 03 15:31:35	03:39:24.90, +00:19:37.43	1.1	0.73	40	4.5	5.1	HR1099	RS CVn
FN8	55625.878	2011 Mar 05 21:03:45	03:36:24.15, +00:31:51.98	0.31	0.21	12	47	29	HR1099	RS CVn
FN9	55510.015	2010 Nov 11 00:21:07	11:40:43.67, -65:01:44.00	0.44	0.35	15	0.27	10	GT Mus	RS CVn
FN10	55769.137	2011 Jul 27 03:16:43	14:34:07.69, -60:33:54.43	0.49	0.32	0	58	8.7	V841 Cen	RS CVn
FN11	55219.255	2010 Jan 23 06:06:55	22:08:29.83, +45:38:19.77	0.64	0.54	75	22	17	AR Lac	RS CVn
FN12	55376.647	2010 Jun 29 15:31:51	22:06:42.49, +45:40:20.19	0.75	0.56	130	19	6.7	AR Lac	RS CVn
FN13	55785.823	2011 Aug 12 19:45:20	22:14:56.90, +46:15:13.01	2.4	0.96	45	0.71	5.2	AR Lac	RS CVn
FN14	55101.059	2009 Sep 28 01:25:30	23:11:50.76, +02:55:10.28	0.53	0.49	15	3.5	5.7	SZ Psc	RS CVn
FN15	55063.937	2009 Aug 20 22:29:55	23:58:33.24, +28:15:57.20	1.1	0.97	45	2.0	19	II Peg	RS CVn
FN16	55291.166	2010 Apr 05 03:58:30	23:54:58.71, +28:51:27.99	0.74	0.64	20	41	13	II Peg	RS CVn
FN17	55433.679	2010 Aug 25 16:17:55	23:55:01.76, +28:36:48.00	1.1	0.7	153	1.2	9.9	II Peg	RS CVn
FN18	55434.315	2010 Aug 26 07:34:00	23:57:52.31, +28:39:34.00	1.2	9.5	0	0.29	9.6	II Peg	RS CVn
FN19	55561.057	2010 Dec 31 01:22:00	03:07:57.26, +40:50:15.00	0.46	0.33	10	20	11	Algol	Algol
FN20	55613.840	2011 Feb 21 20:10:00	20:43:34.04, -32:13:03.96	0.56	0.52	45	69	19	AT Mic	dMe
FN21	55574.278	2011 Jan 13 06:41:00	23:31:33.68, +19:43:53.94	0.35	0.32	40	36	15	EQ Peg	dMe
FN22	55628.897	2011 Mar 08 21:31:00	07:43:46.70, +03:26:26.16	0.32	0.29	160	39	45	YZ CMi	dMe
FN23	55446.767	2010 Sep 07 18:25:00	10:43:41.64, -33:36:30.75	0.57	0.45	150	14	17	TWA 7	YSO

* The time when the maximum luminosity was observed.

† Observed count rate in the 2–10 keV band.

Table 2. General properties of stars in our sample.

Object name	HD	Spectral type	Rotation velocity (km s^{-1})	Radius ($R_\odot$)	a sin$i$* ($R_\odot$)	inclination of orbit (degree)	e	Distance (pc)	References
VY Ari	17433	K3 V + K4 IV§	10.2	1.90	8.2	57	0.085	44	(1)(2)(3)(4)
UX Ari	21242	G5 V + K0 IV§	41.5	5.78	5.9 (h) / 5.3 (c)	59.2	0	50.2	(3)(4)(5)(6)
HR1099	22468	G5 IV + K1 IV§	59.0	3.30	1.9 (h) / 2.4 (c)	38	0	29	(4)(7)(8)(9)(10)
GT Mus	101379	(A0V+A2V) + (G5III+G8III§)	–	33.0	15	10	0.032	172	(4)(11)(12)(13)
V841 Cen‡	127535	K1 IV§	–	3.8	4.1	–	0	63	(14)(15)(16)
AR Lac	210334	G2 IV + K0 IV§	73.7	2.68	4.6 (h) / 4.5 (c)	89.4	0	42	(3)(4)(17)(18)(19)
SZ Psc	219113	F5 IV + K1 IV§	80.2	6.0	8.7 (h) / 6.4 (c)	69.8	0	88	(3)(4)(20)(21)
II Peg	224085	K2 IV§ + M0-3 V	–	2.21	4.9	60	0	42	(4)(22)(23)(24)(25)
Algol	19356	B8 V + K2 IV§	–	3.4	14	81.4	0	28.5	(26)(27)(28)(29)
AT Mic	196982	M4.5 V + M4.5 V§	24.6	0.38	5980	–	–	10.2	(30)(31)(32)(33)
EQ Peg	–	M3.5 V + M5 V§	88.5	0.35	5590	30	–	6.5	(34)(35)(36)(37)(38)
YZ CMi	–	M4.5 V§	5.3	0.29	–	–	–	5.9	(31)(34)(39)
TWA-7	–	M2 V§	19.2	1.89	–	–	–	27	(40)(41)

*The a and i in a sin$i$ show the semi-major axes and inclination angle, respectively. The (h) and (c) show the semi-major axes for the orbit of the hot and cool components, respectively.

§ The stellar component with the symbol § has the largest radius in the multiple-star system. As for the values for the radius and the rotation velocity in this table, the components with this symbol are used.

‡ V841 Cen is a single-lined RS CVn binary.

(1) Alekseev & Kozlova 2001 (2) Bopp et al. 1989 (3) Glebocki & Stawikowski 1995 (4) ESA 1997 (5) Carlos & Popper 1971 (6) Duemmler & Aarum 2001 (7) Donati et al. 1997 (8) Donati 1999 (9) Fekel 1983 (10) Lanza et al. 2006 (11) Murdoch et al. 1995 (12) Randich et al. 1993 (13) Stawikowski & Glebocki 1994 (14) Özeren et al. 1999 (15) Strassmeier et al. 1994 (16) Collier 1982 (17) Chambliss 1976 (18) Zboril et al. 2005 (19) Sanford 1951 (20) Eaton & Henry 2007 (21) Jakate et al. 1976 (22) Berdyugina et al. 1998 (23) Marino et al. 1999 (24) O'Neal et al. 2001 (25) Vogt 1981 (26) Richards et al. 2003 (27) Sarna 1993 (28) Singh et al. 1995 (29) van den Oord & Mewe 1989 (30) Lim et al. 1987 (31) Mitra-Kraev 2007 (32) Mitra-Kraev et al. 2005 (33) Wilson 1978 (34) Morin et al. 2008 (35) Pallavicini et al. 1990a (36) Pettersen et al. 1984 (37) Pizzolato et al. 2003 (38) Hopmann 1958 (39) Reiners et al. 2009 (40) Mamajek 2005 (41) Yang et al. 2008

Table 3: Best-fit parameters in the fitting, and derived flare parameters.

	kT (keV)	EM (10^{54} cm^{-3})	Flux* (10^{-10}ergs cm^{-2} s^{-1})	$L^{\dagger}_{\mathrm{X}(2-20)}$ (10^{31} ergs s^{-1})	χ^2_ν (d.o.f)	$\tau^{\ddagger}_d$ (ks)	$E^{\S}_{\mathrm{tot}}$ (10^{35} ergs)	$l^{\|\|}$ ($\mathrm{R}_\odot$)	$l^{\|\|}$ (binary separation)	$B^{\#}$ (G)
FN1	5	1	2	5	0.42 (4)	26	10	4	0.4	50
	(2–40)	(0.5–2)	(1–3)	(3–7)		(11–50)	(8–20)	(0.1–20)	(0.01–2)	(10–3000)
FN2	4	24	8	20	1.7 (7)	53	100	30	2	20
	(2–30)	(15–36)	(4–10)	(10–30)		(30–81)	(60–200)	(1–100)	(0.1–8)	(8–600)
FN3	$\geq$5	60	40	100	0.63(6)	–	–	$\leq$50	$\leq$4	$\geq$20
		(40–80)	(30–50)	(90–200)		–	–			
FN4	3	100	40	100	0.60 (2)	24	300	100	10	10
	(2–7)	(70–200)	(8–50)	(30–200)		(10–42)	(60–400)	(20–500)	(2–40)	(3–50)
FN5	5	30	30	30	0.42 (5)	6	20	20	3	30
	(3–10)	(20–40)	(10–40)	(10–40)		(4–8)	(5–30)	(5–70)	(0.8–10)	(10–100)
FN6	$\geq$4	3	6	6	0.5 (7)	67	40	$\leq$10	$\leq$2	$\geq$30
		(2–4)	(5–7)	(5–7)		(45–93)	(30-50)			
FN7	$\geq$4	4	8	8	0.76 (3)	–	–	$\leq$10	$\leq$ 10	$\geq$30
		(3–6)	(6–11)	(6–11)		–	–			
FN8	7	30	50	50	0.33 (3)	14	70	20	2	50
	(3–30)	(20–50)	(2–60)	(2–60)		(11–18)	(2–80)	(2–70)	(0.2–10)	(10–500)
FN9	8	160	8	270	1.8 (7)	130	3500	50	0.6	40
	(4–20)	(130–210)	(2–9)	(90–320)		(89–190)	(1200–4200)	(7–600)	(0.1–7)	(5–300)
FN10	$\geq$4	40	20	100	0.19 (3)	7	70	$\leq$60	–	$\geq$20
		(20–60)	(10–30)	(60–200)		(0.1–15)	(3–200)			
FN11	$\geq$6	24	30	60	0.84 (7)	3	16	$\leq$20	$\leq$2	$\geq$50
		(18–31)	(20–35)	(40–70)		(1–4)	(8–23)			
FN12	$\geq$2	30	30	70	1.0 (4)	7	50	$\leq$200	$\leq$20	$\geq$4
		(10–40)	(20–70)	(30–140)		(4–10)	(20–100)			
FN14	$\geq$2	50	6	50	1.2 (8)	72	400	$\leq$300	$\leq$20	$\geq$5
		(30–130)	(4–7)	(40–70)		(49–100)	(300–500)			
FN15	$\geq$8	200	230	500	1.6 (4)	19	900	$\leq$50	$\leq$8	$\geq$50
		(100–300)	(160–420)	(300–900)		(15–24)	(700–2000)			
FN16	3	40	10	25	1.1 (5)	6	14	90	20	10
	(2–7)	(20–60)	(5–20)	(11–32)		(4–8)	(6–20)	(10–300)	(2–50)	(4–70)
FN17	$\geq$7	17	20	40	0.3 (6)	12	50	$\leq$10	$\leq$2	$\geq$60
		(10–23)	(10–40)	(30–80)		(5–43)	(30–160)			
FN18	4	8	4	8	1.3 (3)	41	30	20	3	30
	(2–10)	(4–12)	(0.2–5)	(0.4–10)		(19–97)	(2–60)	(3–70)	(0.5–10)	(8–200)
FN19	–	20	20	30	0.25 (4)	5	10	–	–	–

Table 3: Best-fit parameters in the fitting, and derived flare parameters.

	kT (keV)	EM (10^{54} cm^{-3})	Flux* (10^{-10}ergs cm^{-2} s^{-1})	$L^{\dagger}_{\mathrm{X}(2-20)}$ (10^{31} ergs s^{-1})	χ^2_ν (d.o.f)	$\tau_d^{\ddagger}$ (ks)	$E^{\S}_{\mathrm{tot}}$ (10^{35} ergs)	$l^{\|}$ ($\mathrm{R}_\odot$)	$l^{\|}$ (binary separation)	$B^{\#}$ (G)
	–	(10–30)	(10–40)	(20–60)		(2–9)	(6–30)			
FN20	$\geq$6	2.5	50	6	0.92 (5)	6	3	$\leq$5	–	$\geq$70
		(1.8–3.2)	(30–60)	(4–8)		(4–9)	(2–5)			
FN21	$\geq$4	1.0	40	2	0.54 (4)	4	0.9	$\leq$6	$\leq$0.0005	$\geq$40
		(0.6–1.5)	(30–60)	(1–3)		(2–8)	(0.4–1.7)			
FN22	6	2	70	2.8	1.7 (11)	$\leq$5	$\leq$2	4	–	80
	(3–15)	(1–3)	(30–80)	(1.1–3.3)		–	–	(0.7–20)		(20–400)
FN23	6	20	20	30	0.16 (3)	6	20	20	–	50
	(3–30)	(10–40)	(10–30)	(20–40)		(3–14)	(10–40)	(1–80)		(10–700)

Since statistics are too limited, FN13 is not fitted. Abundances are fixed to the cosmic value, and the absorbing columns are fixed to zero. Errors and lower limits refer to 90 % confidence intervals. The parameters kT, EM, Flux, L_{X} of FN23 (TWA-7) are from Uzawa et al. (2011).

$*$ Flux in the 2–20 keV band.

† Absorption-corrected L_{X} in the 2–20 keV band. Distances are assumed to be the corresponding values in table 1.

‡ *e*-folding time derived with light-curve fitting with a burst model (linear rise and exponential decay).

§ Total released energy derived by multiplying L_{X} by τ_d.

$\|$ Loop length of flare.

$\#$ Magnetic-field strength.

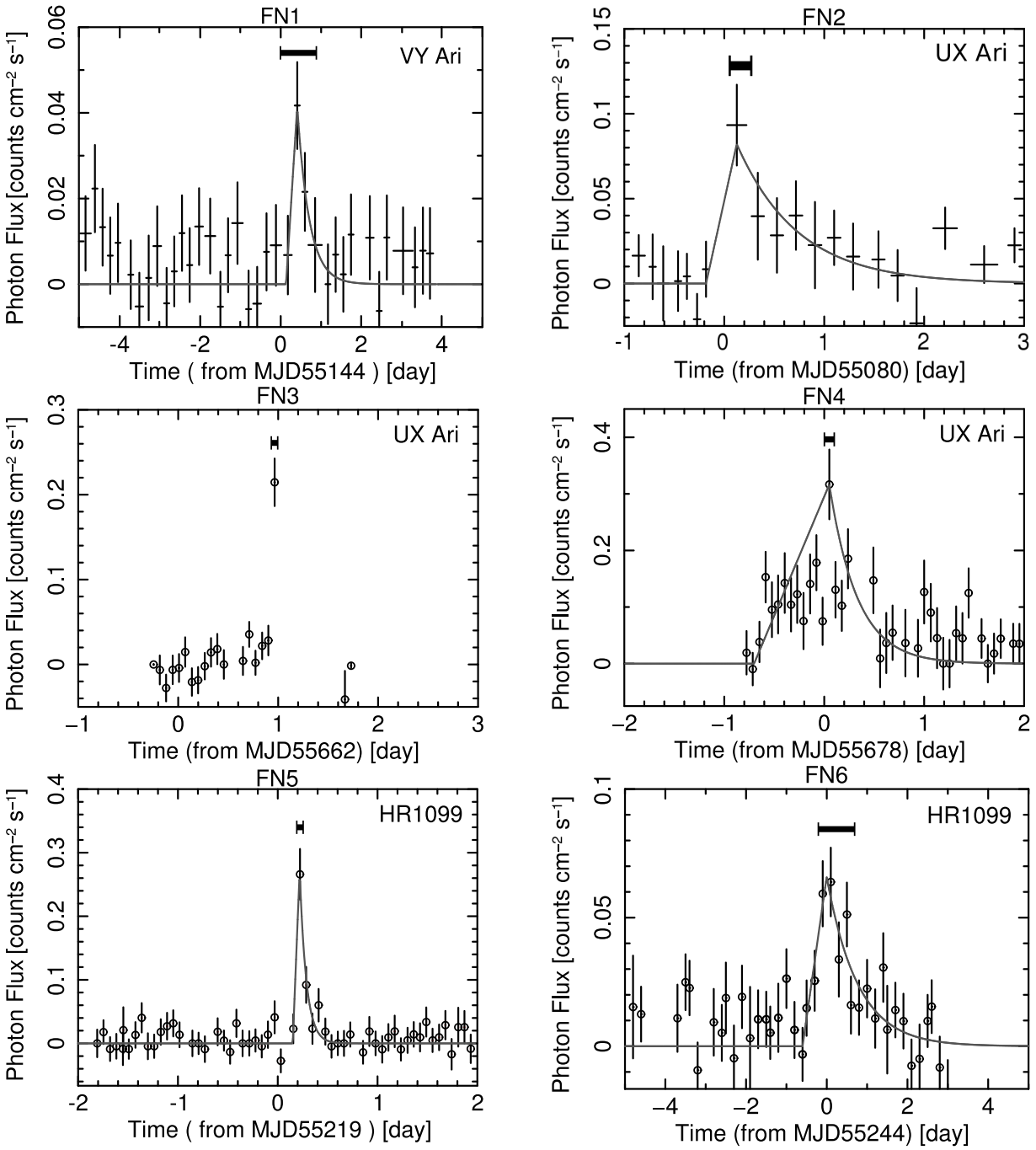
FN1
VY Ari
Photon Flux [counts cm⁻² s⁻¹]
Time (from MJD55144) [day]
FN2
UX Ari
Photon Flux [counts cm⁻² s⁻¹]
Time (from MJD55080) [day]
FN3
UX Ari
Photon Flux [counts cm⁻² s⁻¹]
Time (from MJD55662) [day]
FN4
UX Ari
Photon Flux [counts cm⁻² s⁻¹]
Time (from MJD55678) [day]
FN5
HR1099
Photon Flux [counts cm⁻² s⁻¹]
Time (from MJD55219) [day]
FN6
HR1099
Photon Flux [counts cm⁻² s⁻¹]
Time (from MJD55244) [day]

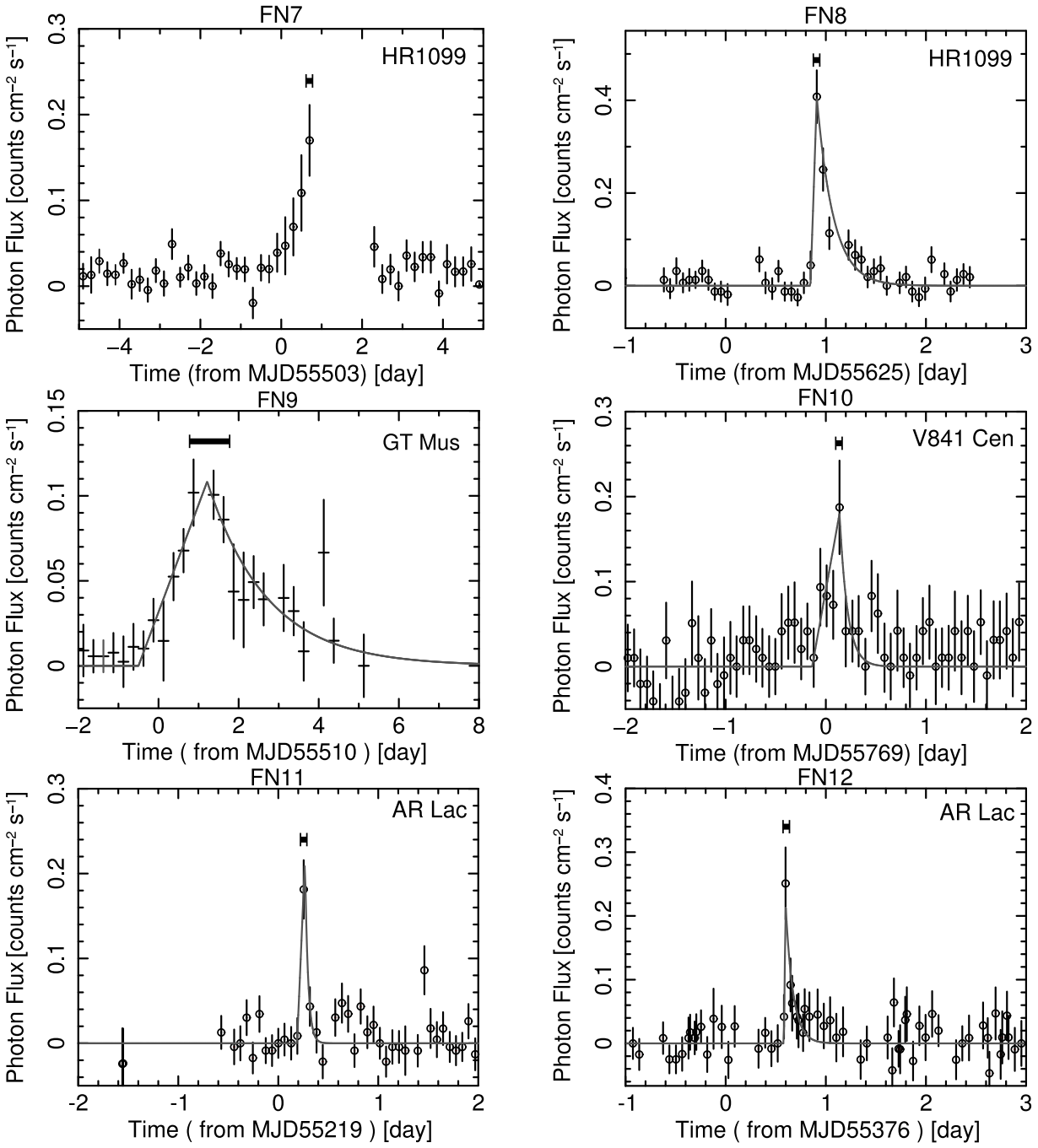
FN7
HR1099
Photon Flux [counts cm⁻² s⁻¹]
Time (from MJD55503) [day]
FN8
HR1099
Time (from MJD55625) [day]
FN9
GT Mus
Time (from MJD55510) [day]
FN10
V841 Cen
Time (from MJD55769) [day]
FN11
AR Lac
Time (from MJD55219) [day]
FN12
AR Lac
Time (from MJD55376) [day]

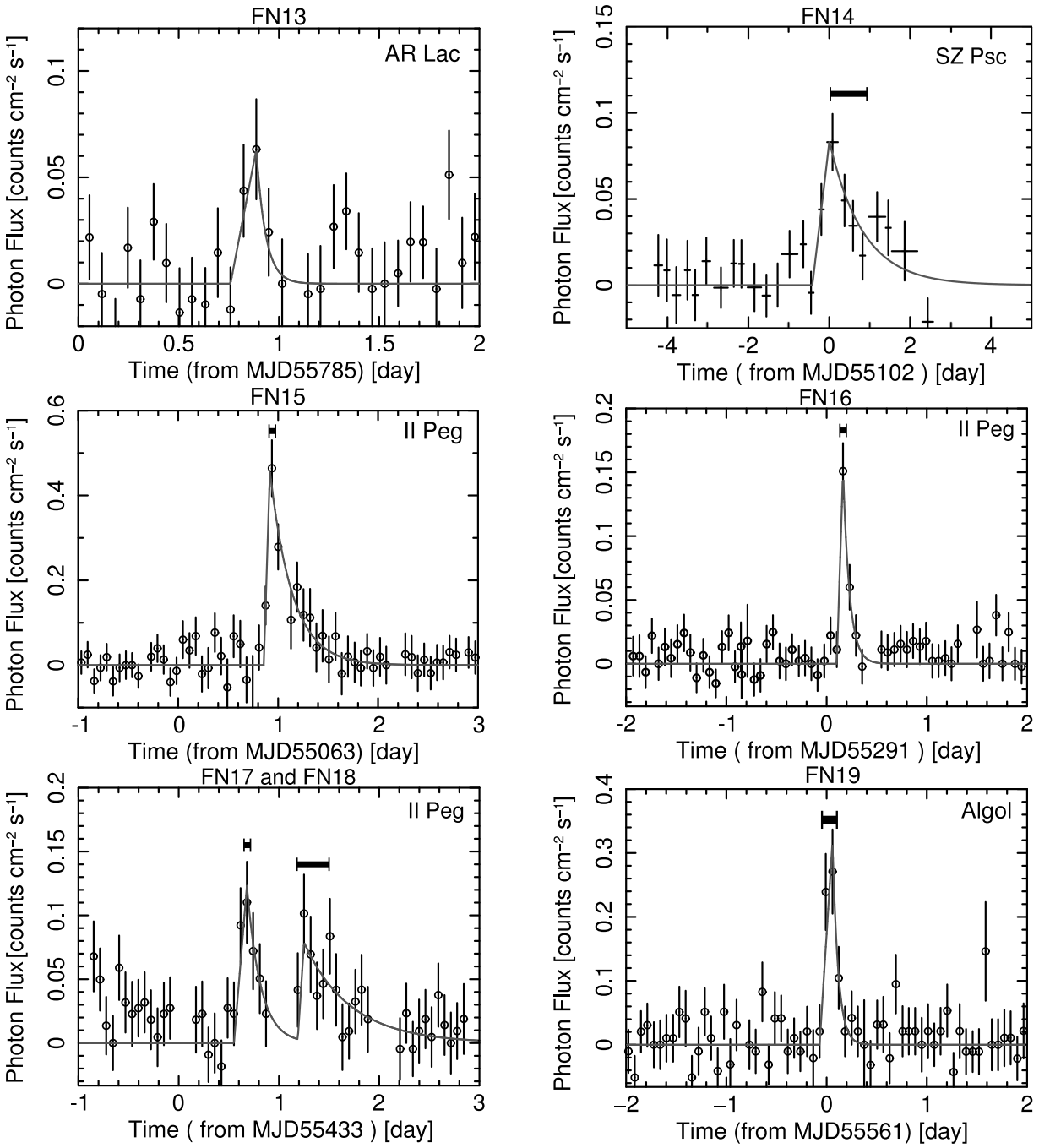
FN13
AR Lac
Photon Flux [counts cm^{-2} s^{-1}]
Time (from MJD55785) [day]
FN14
SZ Psc
Photon Flux [counts cm^{-2} s^{-1}]
Time (from MJD55102) [day]
FN15
II Peg
Photon Flux [counts cm^{-2} s^{-1}]
Time (from MJD55063) [day]
FN16
II Peg
Photon Flux [counts cm^{-2} s^{-1}]
Time (from MJD55291) [day]
FN17 and FN18
II Peg
Photon Flux [counts cm^{-2} s^{-1}]
Time (from MJD55433) [day]
FN19
Algol
Photon Flux [counts cm^{-2} s^{-1}]
Time (from MJD55561) [day]

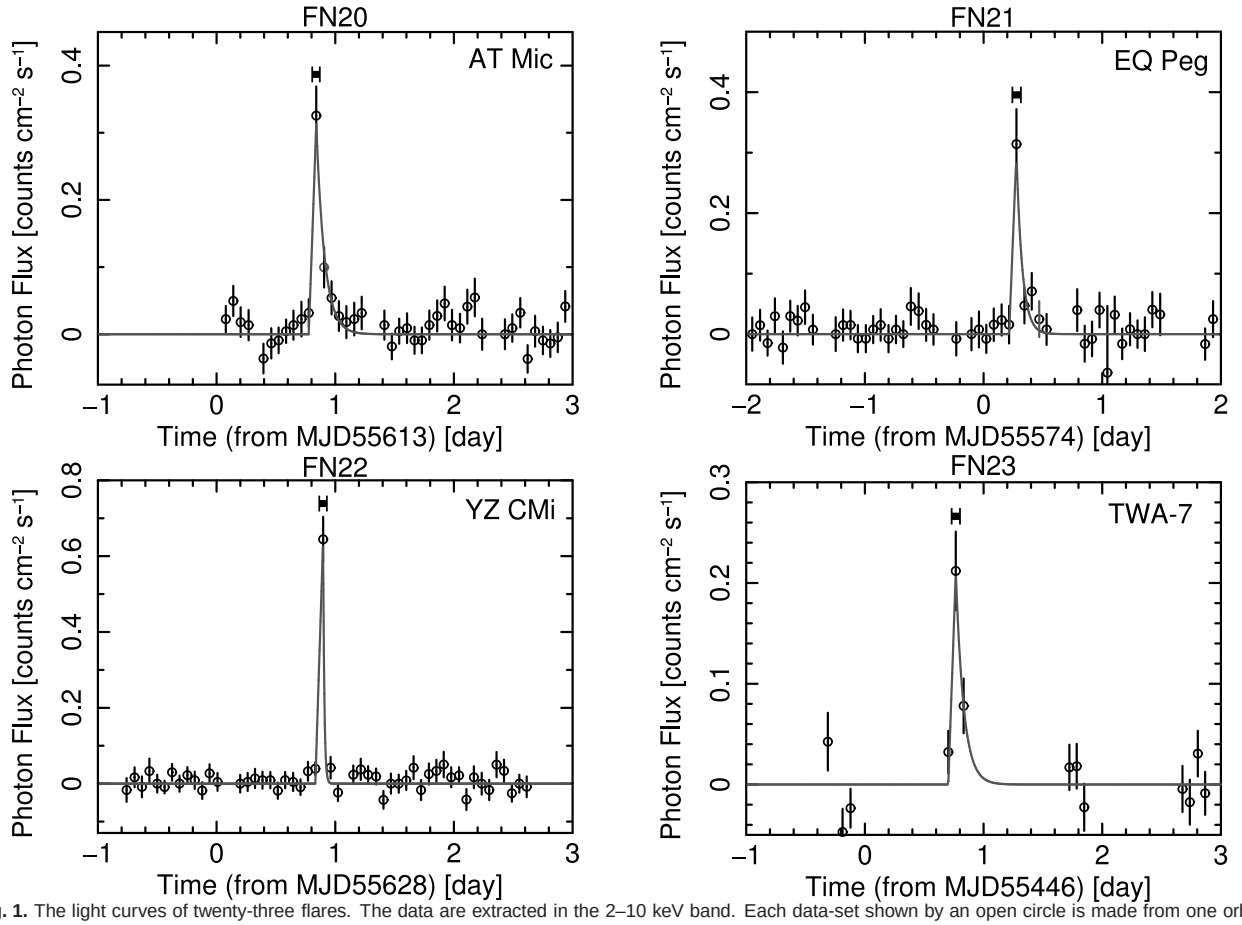

Fig. 1. The light curves of twenty-three flares. The data are extracted in the 2–10 keV band. Each data-set shown by an open circle is made from one orbit data, while the datasets in the panels for FN1, 2, 9 and 14 are binned with the data of multiple orbits. The horizontal bar(s) above the major line peak(s) in each panel is the time interval, from which the data are extracted to derive the detection significances and to make the spectral analysis. The light curve of TWA-7 is from Uzawa et al. (2011).

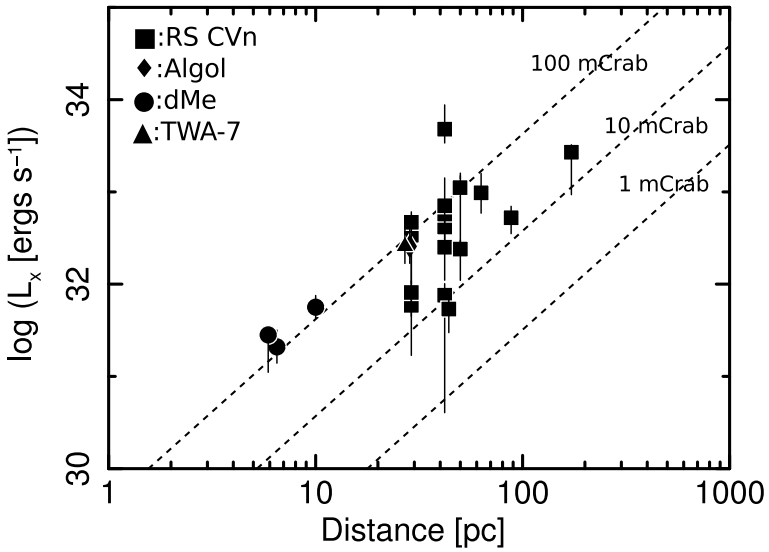

Fig. 2. log-log plot of X-ray luminosity in the 2–20 keV band of flares vs. distance from active stars detected with MAXI/GSC. The filled squares, filled diamond, filled circles and filled triangle show RS-CVn type stars, Algol, dMe stars and TWA-7, respectively. The detection limit appeared to be roughly 10 mCrab in the 2–20 keV band.

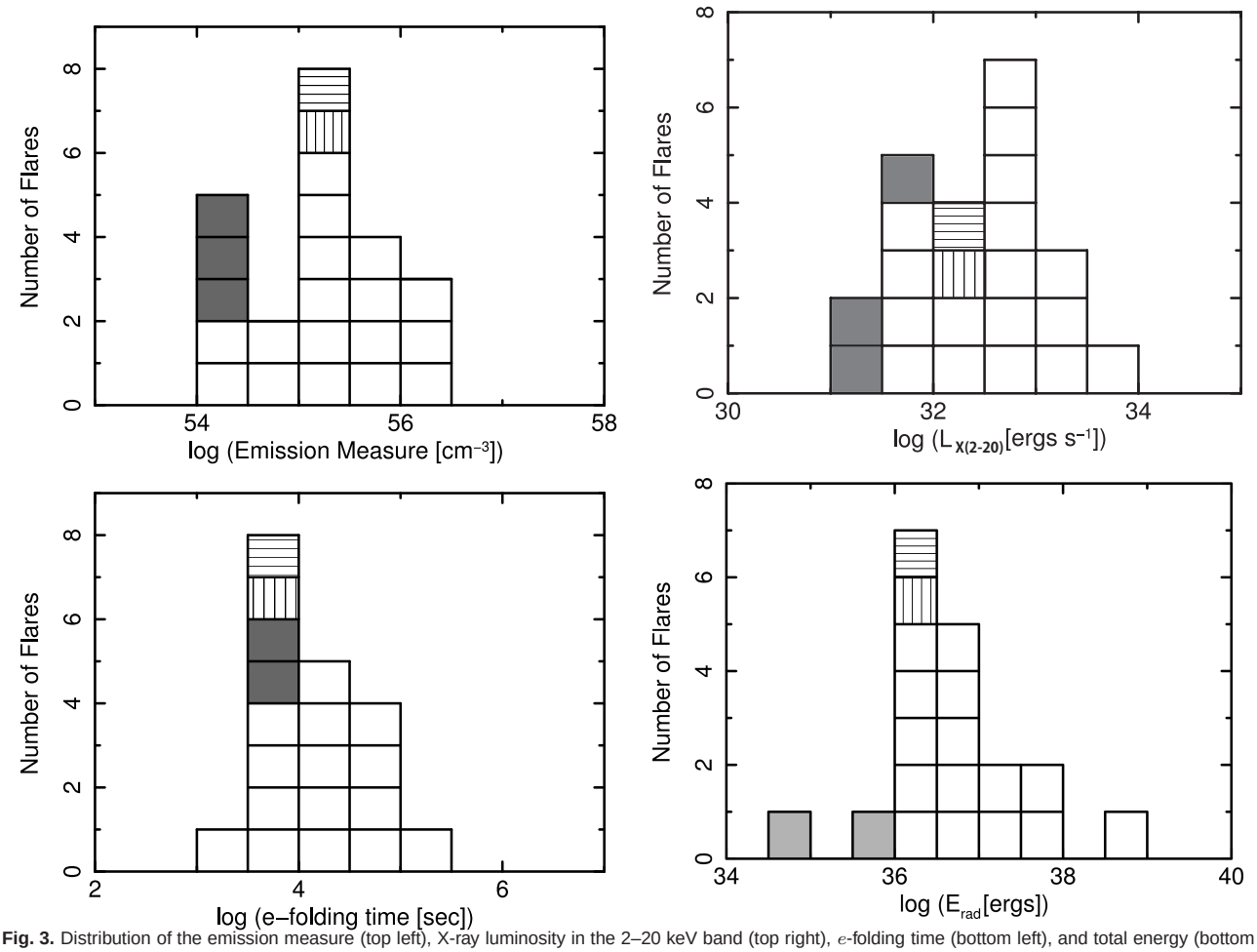

Fig. 3. Distribution of the emission measure (top left), X-ray luminosity in the 2–20 keV band (top right), e-folding time (bottom left), and total energy (bottom right). The open squares, filled squares, vertical-striped square, and horizontal-striped square show RS-CVn type stars, dMe stars, Algol and TWA-7, respectively.

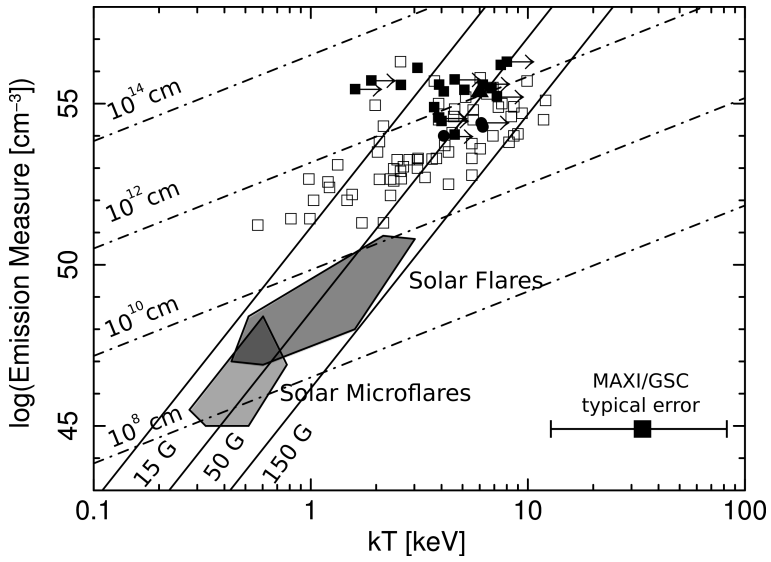

Fig. 4. Log-log plot of emission measure (EM) vs. plasma temperature (kT) for the MAXI X-ray flares (filled symbols, as in figure 2), along with stellar flares from RS-CVn type, Algol, dMe stars and YSOs (open squares; the references given in table 4), solar flares (Feldman et al. 1995), and solar microflares (Shimizu 1995). The arrows indicate the lower limits for individual MAXI/GSC sources. The typical error for MAXI/GSC sources in 90% confidence level is indicated at the bottom-right corner.

The three solid lines are the theoretical EM-kT relation, based on the equation [$EM \propto B^{-5}T^{17/2}$], for B = 15, 50, and 150 Gauss and the four dashed-dotted lines are that based on the equation [$EM \propto l^{5/3}T^{8/3}$] for the loop-sizes of $10^8, 10^{10}$, 10^{12}, and 10^{14} cm (Shibata & Yokoyama 1999).

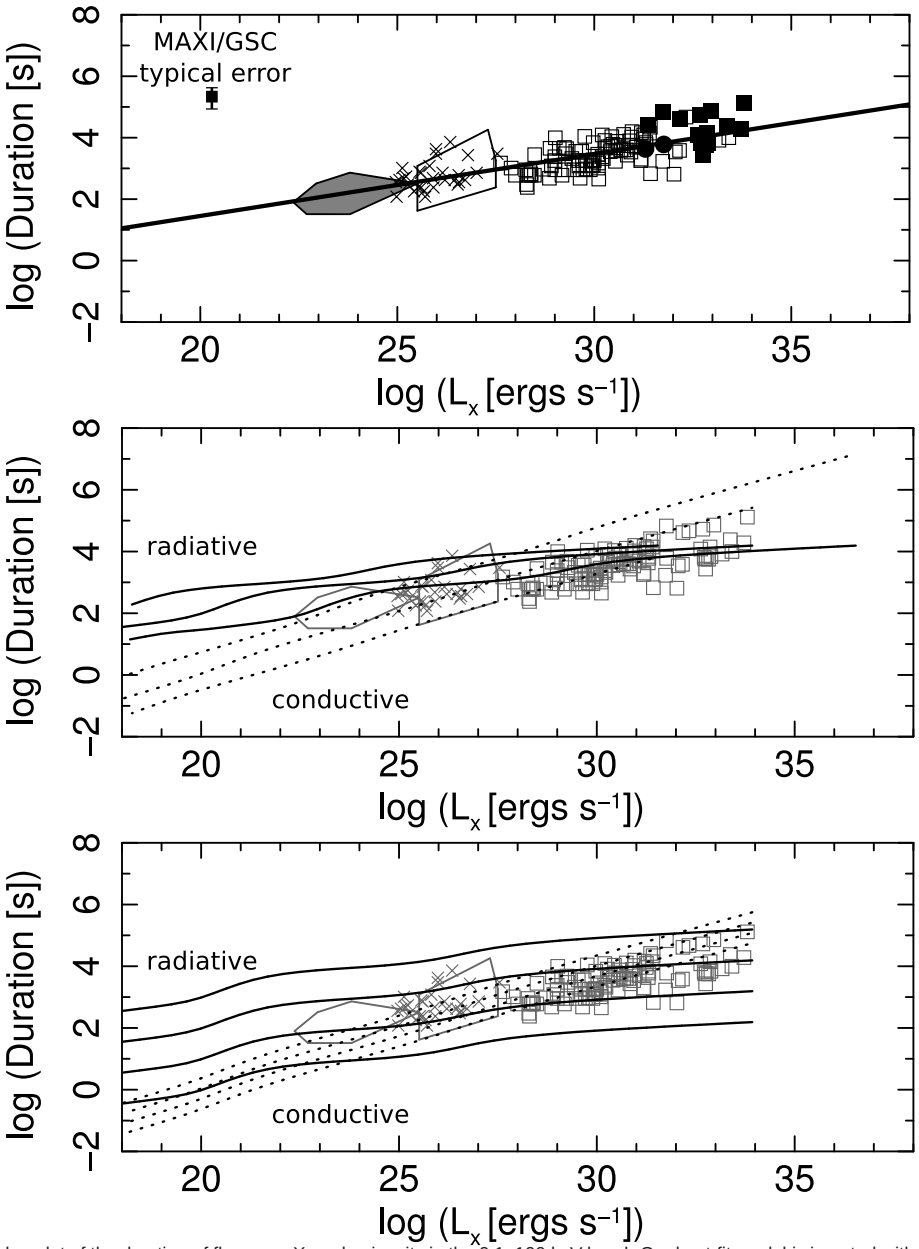

Fig. 5. Top panel: Log-log plot of the duration of flares vs. X-ray luminosity in the 0.1–100 keV band. Our best-fit model is inserted with a broad solid line. The filled and open symbols are the same as those in figure 2 and 4, respectively. We superpose three sets of data of solar flares: X marks, large open pentagon and large gray region, taken from Pallavicini et al. (1977), Veronig et al. (2002) and Shimizu (1995), respectively. The typical error for MAXI/GSC sources is also inserted. Middle panel: The theoretical relations of the radiative cooling model (solid line) and conductive cooling model (dotted line) are overlaid for the non-dimensional parameter α of 0.3, 1 and 3 from the top to bottom lines, respectively, for both the models, where $n_{\rm e}$ is fixed to 10^{11} cm^{-3}. Bottom panel: The same as the middle panel, but with α fixed to 1 and $n_{\rm e}$ varied instead for $n_{\rm e} = 10^{10}$, 10^{11}, 10^{12} and 10^{13} cm^{-3}, corresponding to the 4 lines from top to bottom, respectively, for each model.

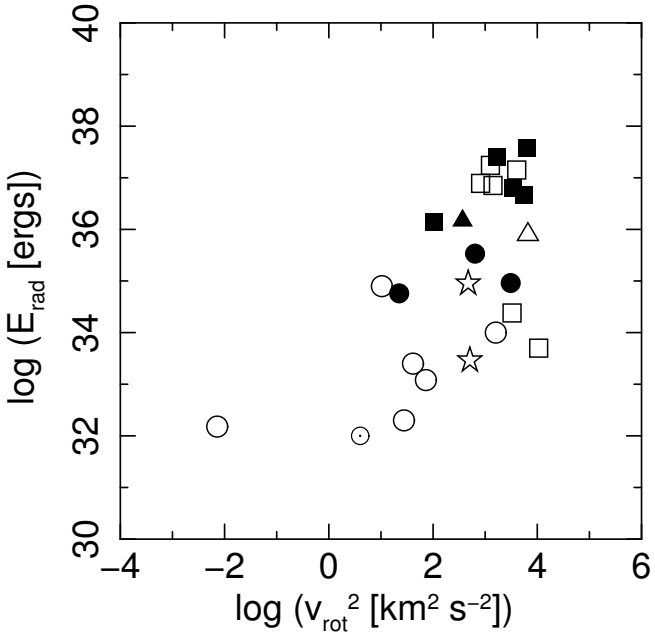

Fig. 6. Log-log plot of total energy released radiatively in a flare vs. the square of rotation velocity. The filled symbols are the same as those in figure 2. The open squares, open circles, open triangles, open stars and open circles with a dot show the values obtained in previous studies for RS-CVn type stars, dMe stars, YSOs, dKe stars and the Sun respectively. If flares have been detected from a source with MAXI or the other missions more than once, only the largest $E_{\rm rad}$ is plotted. For the rotation velocity, if the flare source is a multiple-star system, we used the value of the component which has the largest stellar radius.

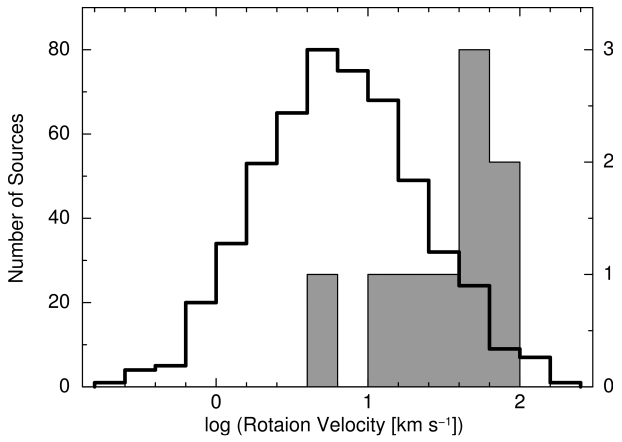

Fig. 7. Histogram of rotation velocities. The gray bars indicate the MAXI/GSC-detected sources within 100 pc with the scale displayed on the right-hand Y-axis. The white bars indicate active binaries and X-ray-detected stellar sources both within 100 pc (from Eker et al. 2008 and Wright et al. 2011), with the scale displayed on the left-hand Y-axis, from which the MAXI/GSC-detected sources are excluded.

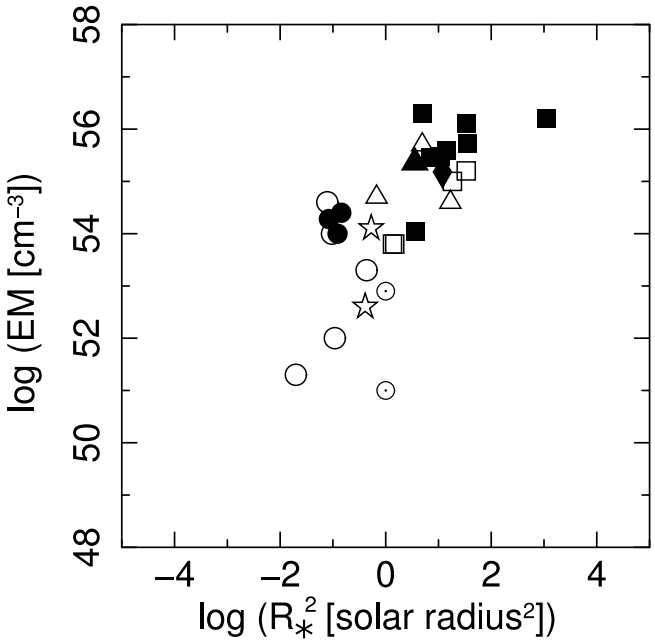

Fig. 8. Log-log plot of emission measure vs. the square of radius. The symbols are the same as in figure 6. The upper open circle with a dot indicates π^1 UMa, while the lower does the Sun.

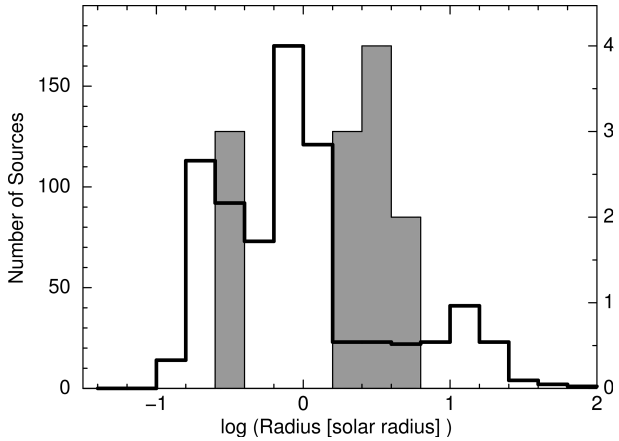

Fig. 9. Histogram of stellar radii. The gray bars indicate the MAXI/GSC sources within 100 pc with the scale displayed on the right-hand Y-axis. The white bars indicate active binaries and X-ray-detected stellar sources both within 100 pc (from Eker et al. 2008 and Wright et al. 2011), with the scale displayed on the left-hand Y-axis, from which the MAXI/GSC-detected sources are excluded.

Table 4. References for figure 4, 5, 6, and 8.

Reference	Figure	Reference	Figure
Alekseev & Kozlova 2001	6	Montmerle et al. 1983	4
Amado et al. 2000	8	Morales et al. 2009	8
Anders et al. 1999	6	Morin et al. 2008	6,8
Benedict et al. 1998	6	Murdoch et al. 1995	8
Bopp et al. 1989	8	O'Brien et al. 2001	6,8
Briggs & Pye 2003	4	O'Neal et al. 2001	6,8
Covino et al. 2001	4,6,8	Osten & Saar 1998	6
Demory et al. 2009	6,8	Osten et al. 2007	5
Dempsey et al. 1993	6	Osten et al. 2010	4,5,6,8
Donati 1999	8	Ottmann & Schmitt 1994	4
Donati et al. 1997	6	Ozawa et al. 1999	4
Doyle et al. 1988	4	Pallavicini et al. 1990a	4,5,6,8
Duemmler & Aarum 2001	6,8	Pallavicini et al. 1990b	4
Eaton & Henry 2007	6,8	Pan & Jordan 1995	4,6,8
Endl et al. 1997	4,6,8	Pan et al. 1997	4,5,8
ESA 1997	5,6	Pandey & Singh 2008	4,5,6,8
Favata & Schmitt 1999	4	Pettersen 1980	6
Favata et al. 2000a	5	Pettersen 1989	8
Favata et al. 2000b	4,6,8	Pizzolato et al. 2003	6
Favata et al. 2001	4,6,8	Poletto et al. 1988	4
Fekel et al. 1999	6,8	Preibisch et al. 1993	4
Franciosini et al. 2001	4,5	Preibisch et al. 1995	4
Frasca et al. 1997	6	Pribulla et al. 2001	6,8
Güdel et al. 1999	4	Pye & McHardy 1983	5,6
Güdel et al. 2004	4,6,8	Qian et al. 2002	8
Gagne et al. 1995	4	Ramseyer et al. 1995	6
Glebocki & Stawikowski 1995	6	Randich et al. 1993	6
Gunn et al. 1998	8	Reiners & Basri 2007	6
Hamaguchi et al. 2000	4	Reiners et al. 2009	6
Hatzes 1995	6	Robinson et al. 2003	6
Huensch & Reimers 1995	4	Sanz-Forcada et al. 2003	6,8
Hussain et al. 2005	6	Singh et al. 1995	6
Imanishi et al. 2001	4	Stawikowski & Glebocki 1994	6
Imanishi et al. 2003	5	Stern et al. 1983	4
Jeffries & Bedford 1990	4,6,8	Stern et al. 1992	5
Kahler et al. 1982	4,6	Strassmeier et al. 1993	6
Kamata et al. 1997	4	Strassmeier et al. 1994	6,8
Kjurkchieva et al. 2000	6	Strassmeier & Rice 1998	6,8
Kovári et al. 2001	6	Strassmeier & Rice 2003	6
Kuerster & Schmitt 1996	4,6,8	Torres & Ribas 2002	6,8
Landini et al. 1986	4,8	Tsuboi et al. 1998	4,5,8
Lim et al. 1987	8	Tsuboi et al. 2000	4
Linsky 1991	5	Tsuru et al. 1989	4
Linsky et al. 2001	8	van den Oord et al. 1988	4,6,8
Maggio et al. 2000	4,5,6,8	van den Oord & Mewe 1989	6,8
Mewe et al. 1997	4	Welty 1995	6,8
Miranda et al. 2007	8	White et al. 1994	8
Mitra-Kraev 2007	6	Wright et al. 2011	6,8
Mitra-Kraev 2007	6	Yang et al. 2008	6,8
Miura et al. 2008	5	Zboril et al. 2005	6,8
Montes et al. 1995	6		

References

Alekseev, I. Y., & Kozlova, O. V. 2001, Astrophysics, 44, 429

Amado, P. J., Doyle, J. G., Byrne, P. B., et al. 2000, A&A, 359, 159

Anders, G. J., Coates, D. W., Thompson, K., & Innis, J. L. 1999, MNRAS, 310, 377

Argiroffi, C., Flaccomio, E., Bouvier, J., et al. 2011, A&A, 530, A1

Benedict, G. F., McArthur, B., Nelan, E., et al. 1998, AJ, 116, 429

Berdyugina, S. V., Jankov, S., Ilyin, I., Tuominen, I., & Fekel, F. C. 1998, A&A, 334, 863

Bopp, B. W., Saar, S. H., Ambruster, C., et al. 1989, ApJ, 339, 1059

Briggs, K. R., & Pye, J. P. 2003, MNRAS, 345, 714

Cargill , P. J., & Klimchuck, J. A. 2004, ApJ, 605, 911

Carlos, R. C., & Popper, D. M. 1971, PASP, 83, 504

Castro-Tirado, A. J., Brandt, S., Lund, N., & Sunyaev, R. 1999, A&A, 347, 927

Chambliss, C. R. 1976, PASP, 88, 762

Christe, S., Hannah, I. G., Krucker, S., McTiernan, J., & Lin, R. P. 2008, ApJ, 677, 1385

Collier, A. C. 1982, Ph.D. Thesis,

Covino, S., Panzera, M. R., Tagliaferri, G., & Pallavicini, R. 2001, A&A, 371, 973

Demory, B.-O., Ségransan, D., Forveille, T., et al. 2009, A&A, 505, 205

Dempsey, R. C., Bopp, B. W., Henry, G. W., & Hall, D. S. 1993, ApJS, 86, 293

Donati, J.-F. 1999, MNRAS, 302, 457

Donati, J.-F., Semel, M., Carter, B. D., Rees, D. E., & Collier Cameron, A. 1997, MNRAS, 291, 658

Doyle, J. G., Butler, C. J., Callanan, P. J., et al. 1988, A&A, 191, 79

Duemmler, R., & Aarum, V. 2001, A&A, 370, 974

Eaton, J. A., & Henry, G. W. 2007, PASP, 119, 259

Eker, Z., Ak, N. F., Bilir, S., et al. 2008, MNRAS, 389, 1722

Endl, M., Strassmeier, K. G., & Kurster, M. 1997, A&A, 328, 565

ESA 1997, ESA Special Publication, 1200,

Favata, F. & Micela, G. 2003, Space Science Reviews, 108, 577

Favata, F., Micela, G., & Reale, F. 2000b, A&A, 354, 1021

Favata, F., Micela, G., & Reale, F. 2001, A&A, 375, 485

Favata, F., Reale, F., Micela, G., et al. 2000a, A&A, 353, 987

Favata, F., & Schmitt, J. H. M. M. 1999, A&A, 350, 900

Fekel, F. C., Jr. 1983, ApJ, 268, 274

Fekel, F. C., Strassmeier, K. G., Weber, M., & Washuettl, A. 1999, A&AS, 137, 369

Feldman, U., Laming, J. M., & Doschek, G. A. 1995, ApJL, 451, L79

Franciosini, E., Pallavicini, R., & Tagliaferri, G. 2001, A&A, 375, 196

Frasca, A., Catalano, S., & Mantovani, D. 1997, A&A, 320, 101

Güdel, M. 2004, A&AR, 12, 71

Güdel, M., Audard, M., Reale, F., Skinner, S. L., & Linsky, J. L. 2004, A&A, 416, 713

Güdel, M., Linsky, J. L., Brown, A., & Nagase, F. 1999, ApJ, 511, 405

Güdel, M., Audard, M., Skinner, S. L., & Horvath, M. I. 2002, ApJL, 580, L73

Gagne, M., Caillault, J.-P., & Stauffer, J. R. 1995, ApJ, 450, 217

Getman, K. V., Broos, P. S., Salter, D. M., Garmire, G. P., & Hogerheijde, M. R. 2011, ApJ, 730, 6

Glebocki, R., & Stawikowski, A. 1995, AcA, 45, 725

Gunn, A. G., Mitrou, C. K., & Doyle, J. G. 1998, MNRAS, 296, 150

Haisch, B., Strong, K., & Rodono, M. 1991 ARAA, 29, 275

Hamaguchi, K., Terada, H., Bamba, A., & Koyama, K. 2000, ApJ, 532, 1111

Hatzes, A. P. 1995, AJ, 109, 350

Hayashi, M. R., Shibata, K., & Matsumoto, R. 1996, ApJL, 468, L37

Hopmann J. 1958, Mitt. Sternw. Wien, 9, 127

Huensch, M., & Reimers, D. 1995, A&A, 296, 509

Hussain, G. A. J., Brickhouse, N. S., Dupree, A. K., et al. 2005, 13th Cambridge Workshop on Cool Stars, Stellar Systems and the Sun, 560, 665

Imanishi, K., Koyama, K., & Tsuboi, Y. 2001, New Century of X-ray Astronomy, 251, 246

Imanishi, K., Nakajima, H., Tsujimoto, M., Koyama, K., & Tsuboi, Y. 2003, PASJ, 55, 653

Jakate, S., Bakos, G. A., Fernie, J. D., & Heard, J. F. 1976, AJ, 81, 250

Jeffries, R. D., & Bedford, D. K. 1990, MNRAS, 246, 337

Kahler, S., Golub, L., Harnden, F. R., et al. 1982, ApJ, 252, 239

Kaastra, J. S. 1992, An X-Ray Spectral Code for Optically Thin Plasmas, (Internal SRON-Leiden Report, updated version 2.0) dd. 12-03-1992.

Kamata, Y., Koyama, K., Tsuboi, Y., & Yamauchi, S. 1997, PASJ, 49, 461

Kastner, J. H., Huenemoerder, D. P., Schulz, N. S., Canizares, C. R., & Weintraub, D. A. 2002, ApJ, 567, 434

Kjurkchieva, D., Marchev, D., & Ogloza, W. 2000, A&A, 354, 909

Kovári, Z., Strassmeier, K. G., Bartus, J., et al. 2001, A&A, 373, 199

Krimm, H. A., Holland, S. T., Corbet, R. H. D., et al. 2013, ApJS, 209, 14

Kuerster, M., & Schmitt, J. H. M. M. 1996, A&A, 311, 211

López-Santiago, J., Montes, D., Crespo-Chacón, I., & Fernández-Figueroa, M. J. 2006, ApJ, 643, 1160

Landini, M., Monsignori Fossi, B. C., Pallavicini, R., & Piro, L. 1986, A&A, 157, 217

Lanza, A. F., Piluso, N., Rodonò, M., Messina, S., & Cutispoto, G. 2006, A&A, 455, 595

Liedahl, D. A., Osterheld, A. L., & Goldstein, W. H. 1995, ApJL, 438, L115

Lim, J., Vaughan, A. E., & Nelson, G. J. 1987, Proceedings of the Astronomical Society of Australia, 7, 197

Linsky, J. L. 1991, Mem. Soc. Astron. Italiana, 62, 307

Linsky, J. L., Skinner, S., Osten, R., & Gagné, M. 2001, Magnetic Fields Across the Hertzsprung-Russell Diagram, 248, 255

Maggio, A., Pallavicini, R., Reale, F., & Tagliaferri, G. 2000, A&A, 356, 627

Mamajek, E. E. 2005, ApJ, 634, 1385

Marino, G., Rodonó, M., Leto, G., & Cutispoto, G. 1999, A&A, 352, 189

Matsuoka, M., Kawasaki, K., Ueno, S., et al. 2009, PASJ, 61, 999

Mewe, R., Gronenschild, E. H. B. M., & van den Oord, G. H. J. 1985, A&AS, 62, 197

Mewe, R., Kaastra, J. S., van den Oord, G. H. J., Vink, J., & Tawara, Y. 1997, A&A, 320, 147

Mewe, R., Lemen, J. R., & van den Oord, G. H. J. 1986, A&AS, 65, 511

Mihara, T., Nakajima, M., Sugizaki, M., et al. 2011, PASJ, 63, 623

Miranda, V., Vaccaro, T., & Oswalt, T. D. 2007, Journal of the Southeastern Association for Research in Astronomy, 1, 17

Mitra-Kraev, U. 2007, The Observatory, 127, 360

Mitra-Kraev, U., Harra, L. K., Güdel, M., et al. 2005, A&A, 431, 679

Miura, J., Tsujimoto, M., Tsuboi, Y., et al. 2008, PASJ, 60, 49

Montes, D., Fernandez-Figueroa, M. J., de Castro, E., & Cornide, M. 1995, A&A, 294, 165

Montmerle, T., Grosso, N., Tsuboi, Y., & Koyama, K. 2000, ApJ, 532, 1097

Montmerle, T., Koch-Miramond, L., Falgarone, E., & Grindlay, J. E. 1983, ApJ, 269, 182

Morales, J. C., Torres, G., Marschall, L. A., & Brehm, W. 2009, ApJ, 707, 671

Morii, M., Kawai, N., Sugimori, K., Suzuki, M., Negoro, H., Sugizaki, M., Nakajima, M., Mihara, T., Matsuoka, M., and The MAXI team 2010, AIP Conf. Proc. 1279, 391

Morin, J., Donati, J.-F., Petit, P., et al. 2008, MNRAS, 390, 567

Murdoch, K. A., Hearnshaw, J. B., Kilmartin, P. M., & Gilmore, A. C. 1995, MNRAS, 276, 836

Negoro, H., Kohama, M., Suzuki, M., et al. 2016 PASJ, 68, S1

Negoro, H., Miyoshi, S., Ozawa, H., et al. 2010, X-ray Astronomy 2009; Present Status, Multi-Wavelength Approach and Future Perspectives, 1248, 589

O'Brien, M. S., Bond, H. E., & Sion, E. M. 2001, 12th European Workshop on White Dwarfs, 226, 240

O'Neal, D., Neff, J. E., Saar, S. H., & Mines, J. K. 2001, AJ, 122, 1954

Osten, R. A., Drake, S., Tueller, J., et al. 2007, ApJ, 654, 1052

Osten, R. A., Godet, O., Drake, S., et al. 2010, ApJ, 721, 785

Osten, R. A., & Saar, S. H. 1998, MNRAS, 295, 257

Ottmann, R., & Schmitt, J. H. M. M. 1994, A&A, 283, 871

Ozawa, H., Nagase, F., Ueda, Y., Dotani, T., & Ishida, M. 1999, ApJL, 523, L81

Özeren, F. F., Doyle, J. G., & Jevremovic, D. 1999, A&A, 350, 635

Pallavicini, R. 1989, A&AR, 1, 177

Pallavicini, R., Serio, S., & Vaiana, G. S. 1977, ApJ, 216, 108

Pallavicini, R., Tagliaferri, G., Pollock, A. M. T., Schmitt, J. H. M. M., & Rosso, C. 1990b, A&A, 227, 483

Pallavicini, R., Tagliaferri, G., & Stella, L. 1990a, A&A, 228, 403

Pan, H. C., & Jordan, C. 1995, MNRAS, 272, 11

Pan, H. C., Jordan, C., Makishima, K., et al. 1997, MNRAS, 285, 735

Pandey, J. C., & Singh, K. P. 2008, MNRAS, 387, 1627

Pettersen, B. R. 1980, AJ, 85, 871

Pettersen, B. R. 1989, A&A, 209, 279

Pettersen, B. R., Coleman, L. A., & Evans, D. S. 1984, ApJ, 282, 214

Pizzolato, N., Maggio, A., Micela, G., Sciortino, S., & Ventura, P. 2003, A&A, 397, 147

Poletto, G., Pallavicini, R., & Kopp, R. A. 1988, A&A, 201, 93

Preibisch, T., Neuhaeuser, R., & Alcala, J. M. 1995, A&A, 304, L13

Preibisch, T., Zinnecker, H., & Schmitt, J. H. M. M. 1993, A&A, 279, L33

Pribulla, T., Chochol, D., Heckert, P. A., et al. 2001, A&A, 371, 997

Pye, J. P., & McHardy, I. M. 1983, MNRAS, 205, 875

Qian, S., Liu, D., Tan, W., & Soonthornthum, B. 2002, AJ, 124, 1060

Ramseyer, T. F., Hatzes, A. P., & Jablonski, F. 1995, AJ, 110, 1364

Randich, S., Gratton, R., & Pallavicini, R. 1993, A&A, 273, 194

Rao, A. R., & Vahia, M. N. 1987, A&A, 188, 109

Reale, F. 2007, A&A, 471,271

Reale, F., & Micela, G. 1998, A&A, 334, 1028

Reiners, A., & Basri, G. 2007, ApJ, 656, 1121

Reiners, A., Basri, G., & Browning, M. 2009, ApJ, 692, 538

Richards, M. T., Waltman, E. B., Ghigo, F. D., & Richards, D. S. P. 2003, ApJS, 147, 337

Riedel, A. R., Finch, C. T., Henry, T. J., et al. 2014, AJ, 147, 85

Robinson, R. D., Ake, T. B., Dupree, A. K., & Linsky, J. L. 2003, The Future of Cool-Star Astrophysics: 12th Cambridge Workshop on Cool Stars, Stellar Systems, and the Sun, 12, 964

Sanford R. F.: 1951, ApJ 113, 299.

Sanz-Forcada, J., Brickhouse, N. S., & Dupree, A. K. 2003, ApJS, 145, 147

Sarna, M. J. 1993, MNRAS, 262, 534

Schaefer, B. E., King, J. R., & Deliyannis, C. P. 2000, ApJ, 529, 1026

Shibata, K., & Yokoyama, T. 1999, ApJL, 526, L49

Shibata, K., & Yokoyama, T. 2002, ApJ, 577, 422

Shimizu, T. 1995, PASJ, 47, 251

Shu, F. H., Shang, H., Glassgold, A. E., & Lee, T. 1997, Science, 277, 1475

Singh, K. P., Drake, S. A., & White, N. E. 1995, ApJ, 445, 840

Smith, R. K., Brickhouse, N. S., Liedahl, D. A., & Raymond, J. C. 2001, ApJL, 556, L91

Söderhjelm, S. 1999, A&A, 341, 121

Stawikowski, A., & Glebocki, R. 1994, AcA, 44, 393

Stern, R. A., Uchida, Y., Tsuneta, S., & Nagase, F. 1992, ApJ, 400, 321

Stern, R. A., Underwood, J. H., & Antiochos, S. K. 1983, ApJL, 264, L55

Strassmeier, K. G., Hall, D. S., Fekel, F. C., & Scheck, M. 1993, A&AS, 100, 173

Strassmeier, K. G., Paunzen, E., & North, P. 1994, Information Bulletin on Variable Stars, 4066, 1

Strassmeier, K. G., & Rice, J. B. 1998, A&A, 339, 497

Strassmeier, K. G., & Rice, J. B. 2003, A&A, 399, 315

Sugizaki, M., Mihara, T., Serino, M., et al. 2011, PASJ, 63, 635

Tomida, H., Tsunemi, H., Kimura, M., et al. 2011, PASJ, 63, 397

Torres, C. A. O., Quast, G. R., da Silva, L., et al. 2006, VizieR Online Data Catalog, 346, 695

Torres, G., & Ribas, I. 2002, ApJ, 567, 1140

Tsuboi, Y., Imanishi, K., Koyama, K., Grosso, N., & Montmerle, T. 2000, ApJ, 532, 1089

Tsuboi, Y., Koyama, K., Murakami, H., et al. 1998, ApJ, 503, 894

Tsunemi, H., Tomida, H., Katayama, H., et al. 2010, PASJ, 62, 1371

Tsuru, T., Makishima, K., Ohashi, T., et al. 1989, PASJ, 41, 679

Uzawa, A., Tsuboi, Y., Morii, M., et al. 2011, PASJ, 63, 713

van den Oord, G. H. J., & Mewe, R. 1989, A&A, 213, 245

van den Oord, G. H. J., Mewe, R., & Brinkman, A. C. 1988, A&A, 205, 181

Veronig, A., Temmer, M., Hanslmeier, A., Otruba, W., & Messerotti, M. 2002, A&A, 382, 1070

Voges, W., Aschenbach, B., Boller, T., et al. 1999, A&A, 349, 389

Vogt, S. S. 1981, ApJ, 247, 975

Welty, A. D. 1995, AJ, 110, 776

White, S. M., Lim, J., & Kundu, M. R. 1994, ApJ, 422, 293

Wilson, O. C. 1978, ApJ, 226, 379

Wright, N. J., Drake, J. J., Mamajek, E. E., & Henry, G. W. 2011, ApJ, 743, 48

Yang, H., Johns-Krull, C. M., & Valenti, J. A. 2008, AJ, 136, 2286

Yokoyama, T., & Shibata, K. 1998, ApJL, 494, L113

Zboril, M., Oliveira, J. M., Messina, S., Djuraševič, G., & Amado, P. J. 2005, Contributions of the Astronomical Observatory Skalnate Pleso, 35, 23